This paper must be cited as:

Ximendes, E.; Benayas, A.; Jaque, D.; Marin, R.; *ACS Nano* 2021, 15, 2, 1917–1941, doi: 10.1021/acsnano.0c08349

Quo Vadis, Nanoparticle-Enabled In Vivo Fluorescence Imaging?

Erving Ximendes[1,2], Antonio Benayas[1], Daniel Jaque[1,2], Riccardo Marin[1]

[1] Fluorescence Imaging Group, Departamento de Física de Materiales – Facultad de Ciencias, Universidad Autónoma de Madrid, C/Francisco Tomás y Valiente 7, Madrid 28049, Spain

[2] Nanobiology Group, Instituto Ramón y Cajal de Investigación Sanitaria, IRYCIS, Ctra. Colmenar km. 9.100, Madrid 28034, Spain

E-mail: riccardo.marin@uam.es

Quo vadis, nanoparticle-enabled in vivo fluorescence imaging?

Erving Ximendes,[a,b] *Antonio Benayas,* [a,b] *Daniel Jaque,*[a,b]* *and Riccardo Marin*[a]*

[a] Fluorescence Imaging Group, Departamento de Física de Materiales, Facultad de Ciencias, Universidad Autónoma de Madrid, C/Francisco Tomás y Valiente 7, Madrid 28049, Spain.

[b] Nanobiology Group, Instituto Ramón y Cajal de Investigación Sanitaria, IRYCIS, Ctra. Colmenar km. 9.100, Madrid 28034, Spain.

KEYWORDS. Fluorescence imaging, nanoparticles, toxicity, tissues, in-vivo imaging, artificial intelligence, light extinction.

ABSTRACT

The exciting developments that we are currently witnessing in terms of novel materials and synthesis approaches is leading to the appearance on the scene of colloidal nanoparticles (NPs) with more and more tunable properties. We have now reached a point where it is possible to synthesize colloidal NPs with functionalities tailored to the needs of society demands. The impact of a wave of new colloidal NPs has been especially important in the field of biomedicine. In that vein, luminescent NPs with improved brightness and near-infrared working capabilities have turned out to be optimal optical probes, capable of fast and high/resolution *in vivo* imaging. However, so far luminescent NPs have shown only a limited portion of their potential. Although we believe that the best is yet to come, the future could be not as bright as some of us might think (and have hoped!). In particular, translation of NP-based fluorescence imaging from preclinical units to the clinics is not that straightforward. In this work, we provide a critical assessment and highlight promising research avenues based on the latest advances in the fields of luminescent NPs and imaging technologies. The disillusioned perspective we herein proffer might sound pessimistic at first, but we consider it necessary to avoid pursuing "pipe dreams" and redirect the efforts towards achievable – yet ambitious – goals.

1. Introduction.

Optical imaging techniques make use of light-matter interaction to garner information about biological systems. This family of diagnostic approaches generates contrast in images capitalizing on different physical mechanisms involving light, such as scattering,[1] absorption,[2-4] conversion to heat,[5] and photoluminescence[6, 7]. Although often endogenous tissue components already provide optical signals, exogenous materials (i.e., contrast agents) are frequently introduced in the biological system to increase contrast.[8-10] The search for suitable contrast agents is indeed a major drive in nanomedicine, along with the development of new approaches capable of localized therapy. These two subfields seamlessly merge in the research area of theranostics, wherein nanoparticles (NPs) combining therapeutic and diagnostic properties are targeted.[11, 12] Whether executed with a theranostic or a contrast agent, the initial step of disease imaging is pivotal to direct the therapeutic efforts and minimize side effects on healthy tissues.[13] Therefore, the development of NPs meeting the requirements of an ideal contrast agent is key. One question arises though: *which are those requirements*? A clear answer to that question affords a stronghold to properly approach the issue of preparing a contrast agent with real potential to be implemented at the clinical level. In this Perspective, we attempt to provide an answer to that question drawing inspiration from recent publications on the use inorganic NP-based contrast agents for *in vivo* fluorescence imaging. In doing so, we highlight the latest trends in the field also pinpointing exciting challenges that lie ahead. Although the discussion focuses on a specific category of contrast agents (inorganic luminescent NPs), many general considerations concerning toxicity and selectivity can be safely extended to any NP to be used in the biomedical realm. Our hope is that the critical assessment of the state-of-the-art presented in this Perspective will support an ever more thought-out design of NP-based contrast agents. This process entails moving away from

some common misconceptions as well as implementing some methodologies that would allow for a smoother transition towards use by physicians. This Perspective has its apex in the identification of the application fields where NP-supported fluorescence imaging can have a real impact (both at clinical and preclinical stage) – a necessary and disillusioned appeal to reason, mainly enforced by the intrinsic physical constraints of the technique.

2. Fluorescence imaging: fundamentals, advantages, and drawbacks.

Fluorescence imaging is based on the use of electromagnetic radiation, within the ultraviolet-visible-near infrared (UV-VIS-NIR) range, emitted by either tissues or exogenous elements. It is used to build up images of cells, tissues, and animals. Although the autofluorescence of tissues can be used itself for bio-imaging, it lacks specificity as different tissues usually show very similar emission spectra, which are located for the most part within the visible range.[14, 15] In addition, the fast attenuation of autofluorescence, caused by the large optical extinction of tissues in the visible, hampers its use for deep-tissue and whole-body anatomical imaging.[16, 17] Alternatively, fluorescence imaging is possible by introducing optical probes (contrast agents) into the specimen to be visualized that can be excited by light (electromagnetic radiation with wavelength ranging from 400 up to 850 nm).[18] The use of this low-energy excitation radiation avoids the intrinsic risks associated with ionizing radiation (mainly alterations of DNA structure).[19] The use of suitable contrast agents allows improving the performance of the different fluorescence imaging modalities, which can be distinguished depending on their specific biomedical aim: anatomical, functional/metabolic, and molecular imaging. [20]

If opting for the use of an exogenous contrast agent, the properties of this optical probe should be tailored to the needs of the specific application. In addition to the use of non-ionizing radiation,

fluorescence imaging shows relevant advantages over other imaging technologies such as magnetic resonance imaging (MRI), nuclear imaging (for instance PET) or computed tomography (CT). These intrinsic advantages of fluorescence imaging are the possibility of real-time imaging and the reduced cost of required equipment. Indeed, fluorescence imaging "simply" requires a fluorescence camera for image acquisition and a laser source for excitation of the tissue or the exogenous contrast agent.

Among the different contrast agents for fluorescence imaging currently being investigated, (small molecules, aptamers, antibodies, peptides, etc.) inorganic fluorescent NPs (from now on simply fluorescent NPs) offer a broad palette of assets.[21] It is feasible to engineer their different physicochemical characteristics and attach diverse functional groups to their surface.[22] Moreover, their small size (below 100 nm) allows them to navigate through the blood stream and enter different organs and tissues, even being interiorized by cells. Fluorescent NPs can absorb the excitation light and re-emit it in a different spectral range. If the NP emission spectrum is significantly different from that of autofluorescence, the fluorescence image can provide reliable information about the location of NPs (with some important caveat as we discuss in **Section 4.2**).[23, 24] Furthermore, the intensity and contrast of the fluorescence image can provide information about the local density of the contrast agent. There are a plethora of luminescent NPs that have been used for *in vivo* fluorescence imaging.[18] Among them, some of the most relevant results have been recently obtained by using rare-earth-based NPs (RENPs), semiconductor nanocrystals (usually referred to as quantum dots, QDs), and carbon-based nanostructures (such as carbon dots -CT- and nanotubes -CNTs). Best results have been obtained when the operating ranges (excitation/emission wavelengths) of these NPs were tuned to fall within the three NIR biological windows (spectral ranges between 750 and 1800 nm where tissues are partially transparent to electromagnetic

radiation – **Figure 1**).[25, 26] It is hence relevant to underscore that NIR-emitting RENPS, CNTs, and QDs were shown to afford *in vivo*, high-resolution and high-contrast whole-body anatomical imaging in small animal models. [27-30]

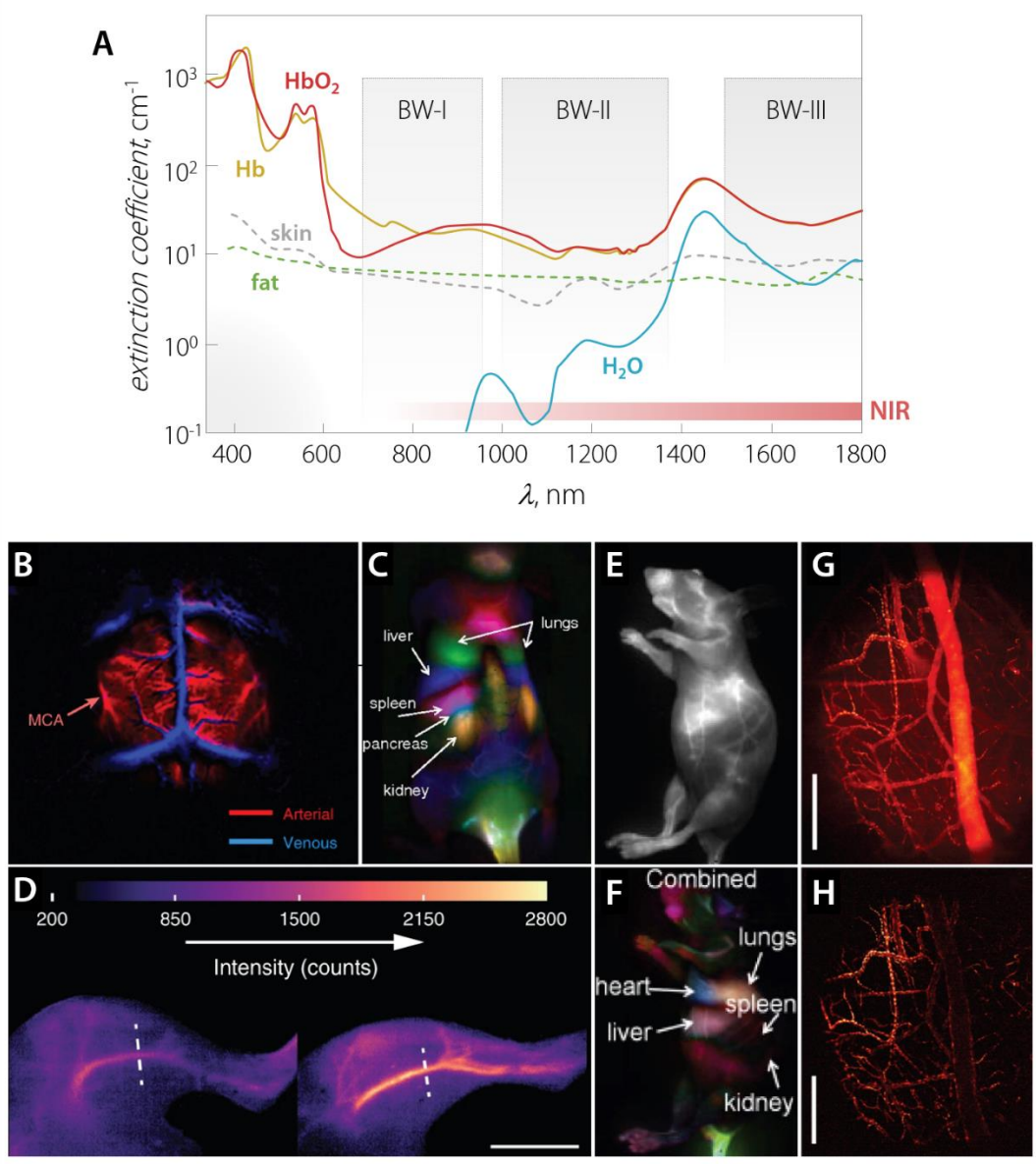

Figure 1. The three biological windows (BWs) and fluorescence anatomical imaging with NIR-emitting NPs. The three BWs all fall in the NIR wavelength range and are delimited by the optical properties of several tissue components (A). The absorption of water and hemoglobin (oxygenated

HbO_2 and de-oxygenated Hb) is shown along with the scattering from skin and fat. The overall extinction that results from the combination of light absorption and scattering from these components (and others) frames three wavelength ranges known as biological (or optical transparency) windows. BW-I: 750- 950 nm, BW-II: 1000-1350 nm, BW-III: 1500-1800 nm. Note that the limits of the BWs are not strictly defined, and often different numbers are reported. The best performance for luminescence imaging contrast agents have been obtained so far with NPs that are excited in BW-I and whose emission falls in BW-II. From B to H different anatomical fluorescence images acquired using NIR-emitting NPs are presented. Cerebral vascular image in the BW-III region with corresponding Principal Component Analysis overlaid showing arterial (red) and venous (blue) vessels of a C57Bl/6 mouse with Er-doped RENPs (B).[31] Reproduced with permission from xxxx. Dynamic contrast-enhanced imaging with CNTs through Principal Component Analysis (C). Reproduced with permission from xxxx. Major features observed belong to the lungs, liver, kidney, and spleen.[27] BW-II fluorescence images (background-corrected) of the left hind limbs of two mice immediately before (top) and after (bottom) intravenous injection of Ag_2S dots (left) or Ag_2S superdots (right).[32] Reproduced with permission from xxxx. BW-II/BW-III fluorescence image of blood flow in the nude mouse after injection of PEGylated Ag_2S QDs (E) and the corresponding Principal Component Analys (F).[33] Reproduced with permission from xxxx. High-resolution, high-speed multicolour angiography images of a glioblastoma tumour through a cranial window using QDs composite NPs (G, H).[34] Reproduced with permission from xxxx.

However, we should be realistic: not all the characteristics of luminescence imaging are advantageous, particularly targeting in vivo applications. The most troublesome one has the form of the Lambert-Beer law. This law describes the extinction of light in a medium as an exponential function, which is even more accentuated through the optically dense biological tissues (both in

the excitation and emission path! – see also **Section 4.2**). This extinction entails both scattering and absorption of photons. This greatly limits the penetration depth achievable with fluorescence imaging inside biological tissues, both in comparison with previously mentioned imaging modalities (MRI, PET, CT) and with optical imaging methods relying on the synergy between diffuse light (scattered) and advanced processing techniques.[35] Therefore, even for small animals, infrared fluorescence imaging-based tomography for the acquisition of 3D images of sufficient resolution appear as a distant dream although first steps are being taken.[36] Yet, in the context of contrast agent-based fluorescence imaging, working in parallel on the fronts of increasing the brightness of the contrast agent's fluorescence signal and its spectral position, a sizeable increase in the achievable penetration depth has been witnessed in the last years (*vide infra*).

3. Degradable NPs: Last advances towards zero toxicity.

The sparkle for this Perspective was ignited by the recent paper by Liu, Hong and co-workers, who reported RENPs with higher solubility in biological environments compared to canonical RENPs such as $NaYF_4$-based NPs (**Figure 2**).[37] $NaREF_4$ NPs are known to undergo degradation upon exposure to aqueous media containing phosphate groups, particularly at low NP concentrations.[38-41] Nevertheless, the new RENPs are composed of K_3ZrF_7, a material whose "soft" crystal lattice imparts superior water solubility to the system. Indeed, the lattice features $[ZrF_7]^{3-}$ units and K^+ ions as building blocks that can be easily solubilized by water. The distorted pentagonal-bipyramidal coordination environment with O_h site-symmetry experienced by Zr^{4+} offers a favorable site for RE^{3+} substitution, given its high coordination number. In the structure, the 7 F^- anions occupy >100 dynamically equivalent positions: a situation that possibly underscore a "fluidity" of the lattice and a high tolerance to defects. In fact, RE^{3+} ions can be doped at high concentration in the structure despite the charge and size mismatch with Zr^{4+}, which is bound to

introduce anion vacancies in the lattice upon substitution. Both near-infrared (NIR) emitting ions (Nd^{3+}/Yb^{3+}) and the iconic upconverting pair Yb^{3+}/Er^{3+} can be doped in the structure,

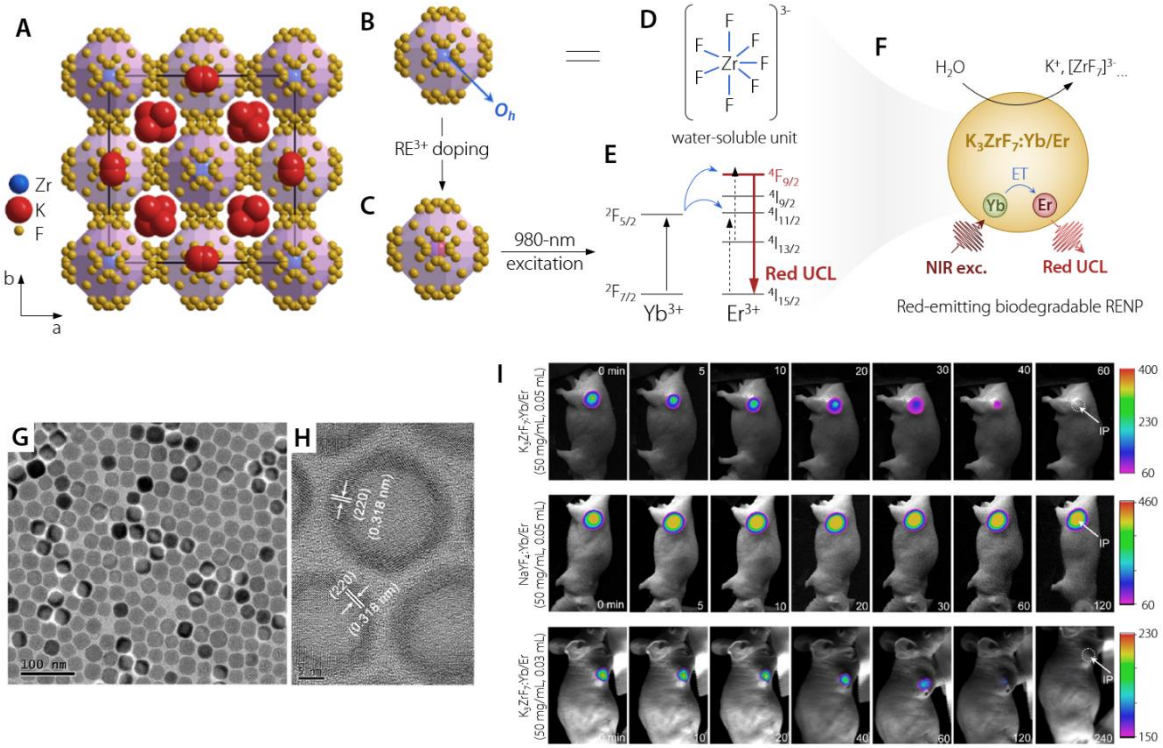

Figure 2. Soluble K_3ZrF_7:Yb^{3+}/Er^{3+} NPs for fluorescence imaging. Crystal structure of K_3ZrF_7 (A) and single $[ZrF_7]^{3-}$ unit, wherein Zr^{4+} occupies a site with O_h coordination environment (B). Doped RE^{3+} ions substitute in this site Zr^{4+} (C). Salient characteristic of the K_3ZrF_7:Yb^{3+}/Er^{3+} NPs are the presence of the water-soluble he $[ZrF_7]^{3-}$ unit (D) and an almost pure red upconversion luminescence (UCL) under 980 nm (E). Combined, these features make these NPs excellent candidates for fluorescence imaging (F). Transmission electron microscopy observation show a highly size monodisperse sample (G) with good crystallinity (H). The *in vivo* dissolution of the NPs after subcutaneous administration was followed monitoring the emission intensity versus time, and comparing it to the trend observed for $NaYF_4$:Yb^{3+}/Er^{3+} NPs (I). Adapted with permission from xxxx.

thus yielding downshifting or upconversion emission under NIR excitation within BW-I and BW-II. Importantly, both high and low pH values prompt dissolution of the RENPs at a fast rate; a behavior observed also after dispersion of the hydrophobic RENPs in peanut oil and subcutaneous injection in mice. The dissolution within animals was followed spectroscopically as well as via mass spectroscopy on collected excretions and harvested organs. The observed almost complete excretion of the solubilized material drastically reduces the risk of toxicity due to accumulation of particles or ions (Zr^{4+} in this case) at specific organs, such as lungs and liver. At the same time, the upconversion emission was observed up to 2 h post-injection: a time span sufficient to perform imaging. Despite the relevance of the results published by Liu, Hong and co-workers, the potential application of their visible emitting NPs for *in vivo* imaging is limited due to the strong tissue extinction in this spectral range (**Figure 1A**). This limitation could be easily overcome by adequate choice of RE ions. For instance, as already proposed by the authors of the study, one can move from the Er/Yb pair to Nd/Yb: this allows shifting the emission wavelength from the visible to BW-II. This yields a nanostructure capable of deep-tissue, *in vivo* imaging and soluble in biological environments.

These RENPs, that diligently vanquish after they have done their job as contrast agents, constitute a step along the right direction of future efforts in the research on fluorescence imaging for *in vivo* applications. Indeed, these RENPs address one main concern linked to the use of NPs in biomedicine generally speaking: their long-term toxicity owing to accumulation in organs.[42]

Achieving dissolution of the NPs is one way to approach the issue of accumulation. Clearly, this strategy only works for NPs whose dissolution products exhibit negligible toxicity. However, most of the NPs investigated for biomedical applications are far less soluble in biological media and/or leached ions can be cytotoxic (e.g., Ag^{+} and Cu^{2+}).[43, 44] Moreover, an extended circulation time is

usually required to allow accumulation of the NPs at the tissue of interest (to be imaged or treated). And, indeed, strategies have been developed to make NPs more stealth (i.e., biomimetic) so to avoid premature uptake from macrophages (*vide infra*). In those instances, it is beneficial to further limit the NP dissolution (via suitable surface coatings) and rely on their clearance. Intravenously administered NPs usually undergo elimination mainly via renal (smaller NPs, < 5.5 nm) and hepatobiliary elimination (larger NPs).[45, 46] The former mechanism is better understood than the hepatobiliary pathway; thus, future efforts should be devoted to increase our understanding of the complex mechanisms underpinning the latter. To that end, a recent study from Chan and co-workers has investigated specifically the barriers encountered by model NPs (gold nanoparticles) of different sizes during hepatobiliary elimination after intravenous injection (**Figure 3**).[47] Combining their results with previous literature, they highlighted the prominent role played by Kupffer and liver sinusoidal endothelial cells in reducing the effectiveness of this form of NP excretion. The authors observed that both types of cells are capable of strongly interact with NPs due to high phagocytic ability towards them. In order to enhance clearance through this hepatobiliary elimination, NPs should therefore be engineered to minimize the interaction with these cells, which constitute the *first line of defense* of the liver.

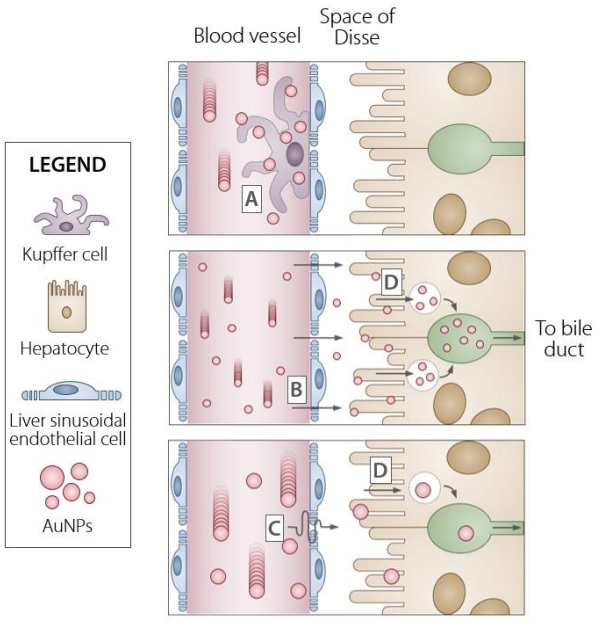

Figure 3. Mechanism of hepatobiliary elimination for non-soluble NPs in the liver sinusoid proposed by Chan and co-workers.[47] The authors suggest that, after intravenous injection, the NPs enter the liver and they get subsequently uptaken by Kupffer cells in the liver sinusoid (A). The larger circulating NPs are sequestered more easily, while smaller NPs cross the sinusoidal endothelium (B). Upon removal of the Kupffer cells, the larger NPs can also more easily extravasate. However, the fenestrae size limit of the liver sinusoidal endothelial cells can hinder this process (C). Lastly, the NPs accumulate at the space of Disse, where hepatocytes take them up, favoring the NP transport into the bile canaliculus (D). The final step is constituted by the transit of the NP outside the liver and into the intestine, from where they are eventually expelled from the body through the feces. Adapted with permission from xxxx.

---

4. Characteristics of a NP-based fluorescence imaging contrast agent.

In a more holistic way, there are several points that one should consider when designing NPs for biomedical use, and some of them are specific to the case of NP-based fluorescence imaging

contrast agents. To that end, in this Perspective we identify the following aspects as the most important ones to take into account, and that should drive future experimental efforts in the field:

- **Toxicity**: this is a rather broad and multifaceted issue, and control over it entails attention to the composition of the constituent material, NP surface chemistry, and size/ morphology;

- **Specificity**: the NP should bind as specifically as possible to the targeted tissue, aiming for a "magic bullet"-like type of properties and overcoming possible physical barriers within the body;

- **Range of excitability and emission**: light of specific wavelengths interact less with the constituents of tissues, thus affording deeper penetration within the human body as well as less spectral distortion;

- **Brightness**: fixed the excitation and emission wavelength, the more photons are emitted per photons shined on the NP, the more effective is the contrast agent since it could afford higher penetration depth, contrast, and resolution (both spatial and temporal).

The next sections will specifically deal with these aspects, reviewing those we believe have been the highlights in the past years, and suggesting future directions of investigation.

4.1 Minimizing toxicity and immune response, while enhancing specific targeting.

Human beings did not invent nanoparticles. In nature, they could be found in dust, sand, volcanic ashes, and even in some biological entities like magnetotactic bacteria or viruses (which are nanosized themselves).[48-51] However, the anthropogenic activity has led to an increased presence

of nanoparticles in the environment, which translates to a heavier exposure to a greater variety of materials. Before the era of nanotechnology, NPs were rather grouped with larger sub-micrometric materials in the broader category of ultrafine particles (UFPs), a term still used in toxicology to refer to this class of tiny materials. Therefore, although the term nanotoxicology appears in the literature between the years 2003/2004,[52-54] concerns and studies about the effect of NPs (or UFPs) on health predate the coinage of this word.[55-58] Exposure to NPs in nature mainly occurs via inhalation, and from the tissue of the upper and lower respiratory tract they can enter the blood stream and/or translocate to other systems.[59-61] NPs can enter the body also via skin contact (e.g., sunscreen) and oral ingestion, and the advent of nanomedicine will result more consistently in the direct injection of NPs in the body.[62] The latter exposure route is the one more likely to be of interest in the framework of fluorescence imaging for *in vivo* applications, and has been shown to pose higher risks connected to the accumulation.[63] Importantly, once the NPs are in the blood stream and/or accumulated at the site of interest, they can elicit an immune response. This side effect is clearly to be avoided; but what are the features of a NP that can play a role in this context? Several studies have been published in the past couple of decades, which have highlighted the effect of the NP composition, size, morphology, and surface chemistry/charge in the human body (**Figure 4**). Before delving into these aspects, it is important to mention that it is not always easy to investigate their effects separately, owing to the difficulty to carry out the investigation *ceteribus paribus* (i.e., all other conditions fixed).[63] While this is somehow possible in the frame of a single study, it is almost impossible to compare the results obtained in different investigations carried out around the world.

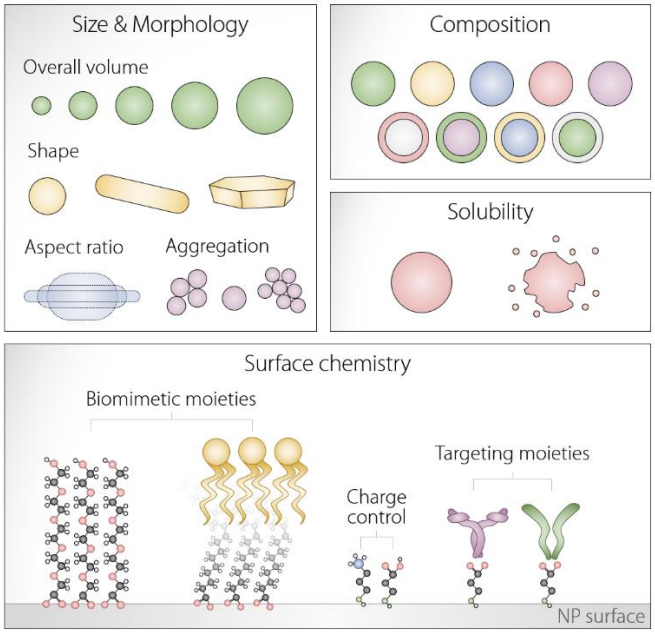

Figure 4. Summary of the most relevant parameters for the toxicity of nanoparticles. This summary is not intended to be comprehensive, but it rather provides the reader at a glance with the most important aspects that influence the toxicity and, more in general, the interaction of a NP with biological entities.

This is due to the lack of standardization in the assessment of the toxicity of nanomaterials, and the inherent difficulty in controlling in a fully reproducible way the properties of the materials at that scale on a batch-to-batch scale. Setting standards in terms of procedures and parameters reported in each study is of utmost importance to advance the knowledge in the field of nano-biotechnology.[64-66] To that end, Caruso, Crampin and co-workers have already proposed guidelines for minimum information reporting in bio-nano experimental literature (MIRIBEL), openly encouraging "*the bio–nano science community to adopt a 'reporting standard' to enhance the quality and reuse of published research*".[67] Following such guidelines should become the praxis for a more impactful and relevant advancement of our knowledge.[68] We argue that also an

effort of screening at the editorial level the compliance to this good practice will be most beneficial in this regard.

Before starting discussing more in detail the aspects regarding toxicity, stealth properties, and targeting ability, we should point out how the use of artificial intelligence is emerging as a powerful tool to predict the toxicity[63, 69] and fate[70] of NPs possessing different composition, size, morphology, and surface chemistry (**Figure 5**). The use of these neural networks requires large amounts of data as a training set to then be able and predict reliably the behavior of a NP. Therefore, the identification of a minimum set of parameters to be provided in studies focusing on the biomedical application of NPs (and that can be used to feed the learning algorithm) is key also to support the advancement of this predictive tool. As we detail further towards the end of this Perspective, we believe that the contribution of artificial intelligence to the future of luminescence imaging does not end here.

4.1.1. Chemical composition. Since 2003, Europe has banned heavy metals from most vehicle components[71] and the extension of this ban to electronic devices has been on the table for a long time now.[72] Along with mercury and hexavalent chromium, cadmium and lead are on the blacklist; coincidentally, they are amongst the most used metals for producing highly efficient QDs. Cd-based QDs are the benchmark in terms of luminescence intensity in the visible part of the spectrum, with photoluminescence quantum yields (PLQYs, # of emitted photons per # of absorbed photons) approaching unity.[73] PbS QDs, and even more so in their PbS/CdS core/shell form, are of particular interest for *in vivo* biomedical applications owing to their brightness and NIR working capabilities, which ensure better penetration depth (*vide infra*).[74] Admittedly, exceptions to the ban have been introduced, due to technological limitations that prevent obtaining the same standards achievable

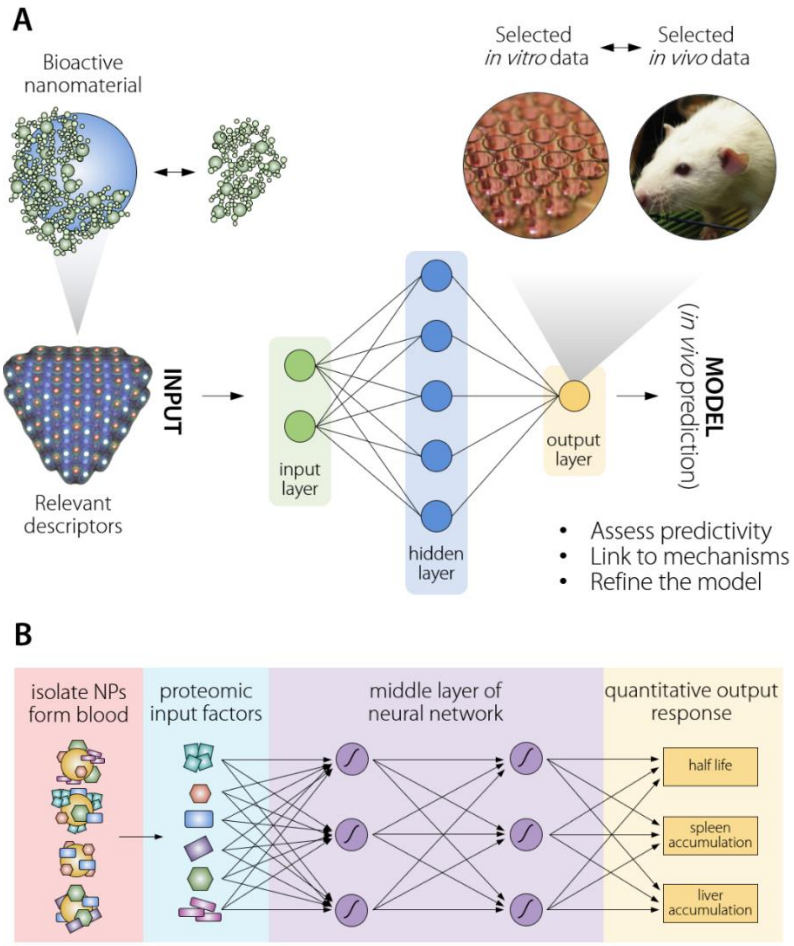

Figure 5. Artificial intelligence to predict the toxic effect and fate of NPs. Scheme of the QSAR (quantitative structure-activity relationship) method as summarized by Winkler et al. (A).[69] The most relevant molecular descriptors of the bioactive form of NPs (i.e., coated with biological molecules upon interaction with the environment) are identified. The neural network is trained with this input of descriptors, along with *in vivo* and/or *in vitro* data. These datasets can also be used to generate a statistical regression model. Using the validated model, properties of new nanomaterials can be predicted, as well as biological mechanisms and processes. Adapted with permission from xxxx. Scheme of the approach developed by Lazarovits et al. for the prediction of the fate of NPs *in vivo* (B).[70] After intravenous injection of different gold NPs in mice, the NPs were isolated from blood and the proteins adsorbed on the surface identified and quantified via mass spectrometry. These data were used to train along with quantitative information on the

accumulation of the NPs at different organs (also obtained via mass spectrometry). After training and validation, the neural network could predict the behavior of unknown NPs. Adapted with permission from xxxx.

---

with materials and processing techniques involving heavy metals.[75] However, it is natural to think that, if heavy-metal-containing QDs have an uncertain future in a number of technological fields, it is highly unlikely that similar NPs will work their way in the to the clinical practice. One of the main issues is in the possibility of metal ion leaching within the body. One might argue that the total amount used is generally small (see **Table 1**). Hence the benefit of an accurate detection leading to a reliable diagnosis should greatly outweigh the risks associated with the toxicity of the contrast agent. However, at times it is necessary to repeat the imaging procedure more than once to assess the development of the disease or the efficacy of the treatment. Cumulative effects can therefore come into play. Moreover, the disposal of heavy-metal-contaminated material is a problem, both at the level of NP production and after (possible) use at clinical level, posing a threat mainly to aquatic life and soil.[76] Therefore, heavy-metal-free NPs are to be preferred over classical, Cd- and Pb-based QDs. (Ag,Cu)In(S,Se,Te)$_2$ (even though Ag^+ and $Cu^{+/2+}$ are also cytotoxic, as mentioned above[43, 44]), InAs, InP, and Ag_2S are possible candidates as far as QDs (or semiconductor nanocrystals more broadly speaking) are concerned. Regarding the other class of potential candidates for luminescence imaging, RENPs with a real potential to be used in biomedical applications are usually based on fluorides or oxides, and often contains alkaline metals. While alkaline metal ions can be considered safe, the toxicity of RE^{3+} ions is debated, but they are generally considered less toxic than heavy metals.[77, 78] Toxicity of RE^{3+} is a matter of

concern particularly due to exposure in the workplace via inhalation.[77] Nonetheless, further studies have shown that continuous

Table 1. Selection of studies where Pb-containing QDs were used as contrast agents for fluorescence imaging. Reported parameters are from left to right the material composition, maximum of the emission spectrum (λ_{em}^{max}), photoluminescence quantum yield (*PLQY*), surface chemistry, mouse type, injection modality (r.o.=retroorbital, i.v.=intravenous, s.c.=subcutaneous), concentration of the injected suspension, total volume injected, and the total injected mass of QDs. PbS QDs were selected as representative of heavy metal-containing NPs working in the NIR range, where biological tissues are more transparent (see **Section 4**).

Material	$\boldsymbol{\lambda_{em}^{max}}$**, nm**	***PLQY*, %**	***Surface***	***Mouse***	***Injection***	***Conc.*, mg/mL**	***Volume injected*, µL**	***Total mass*, mg (mg/kg)[a]**	**Ref.**
PbS/CdS/ZnS	1270	*NA*	Mercaptopropionic acid	Female CD1	r.o./i.v.	0.04	100	0.004 ($1.3\cdot10^{-4}$)	[74]
PbS/CdS	1650	2.2-22%	Oleyamine-branched polyacrylic acid + PEG	Female C57BL/6	i.v.	2	200	0.4 ($1.3\cdot10^{-2}$)	[79]
PbS	1300	20.30%	β-lactoglobulin	Female nude	i.v.	0.25	200	0.05 ($1.7\cdot10^{-3}$)	[80]
PbS:Zn^{2+}	1630	up to 50%	oleyamine-branched polyacrylic acid + PEG	Balb/C	i.v.	6	100	0.6 ($2\cdot10^{-2}$)	[81]
PbS	903	*NA*	silica PEG	Male nude	s.c.	1	30	0.03 ($1\cdot10^{-3}$)	[82]
PbS	900	*NA*	1,2-Diacyl-sn-Glycero-3-PhosphoethanolamineN-[Methoxy(Polyethylene glycol)] (mPEG-DSPE)	Balb/C	i.v.	*NA*	*NA*	($2.5\cdot10^{-2}$)[b]	[83]
PbS	1308	17.3	RNase	Nude	i.v	26 nM	200	0.001 ($3.3\cdot10^{-5}$)	[84]
PbS	1050-1220	*NA*	dihydrolipoic acid–polyethylene glycol	*NA*	i.v.	0.01	30	0.0003 ($1\cdot10^{-5}$)	[85]
PbS/CdS/ZnS	1026, 820 (UC)[c]	4.6 (UC)[c]	1,2-Diacyl-sn-Glycero-3-PhosphoethanolamineN-[Methoxy(Polyethylene glycol)] (mPEG-DSPE)	Nude	s.c.	3	30	0.09 ($3\cdot10^{-3}$)	[86]

[a] In parentheses we report the mass of NP normalized to the weight of the animal considering a body weight of 30 g for all animals.
[b] Value obtained from the toxicity tests rather than from imaging.
[c] The produced QDs displayed upconversion (UC) emission.

exposure via ingestion or injection also has negative effects, with damages induced to various organs (liver, kidney, heart, brain). This is far from unexpected, since RE^{3+} ions are often used as catalysts in many reactions and they are known to interact with biological molecules,[87] likely being also able to act as substrate for unwanted reactions.

To prevent metal ion leaching from NPs, for both QDs and RENPs a protective shell of inert material can be grown on their surface: a strategy that has usually the advantage of also increasing the emission brightness of the luminescent NP. ZnS[88] and CaF_2[89] are two exemplary materials that do not contain toxic elements for shelling QDs and RENPs, respectively. It has also been recently demonstrated how ultrafast laser irradiation can be used to build a protective layer on Ag_2S NPs, ultimately resulting in an increased luminescence brightness while keeping the toxicity at minimum (**Figure 6**).[32]

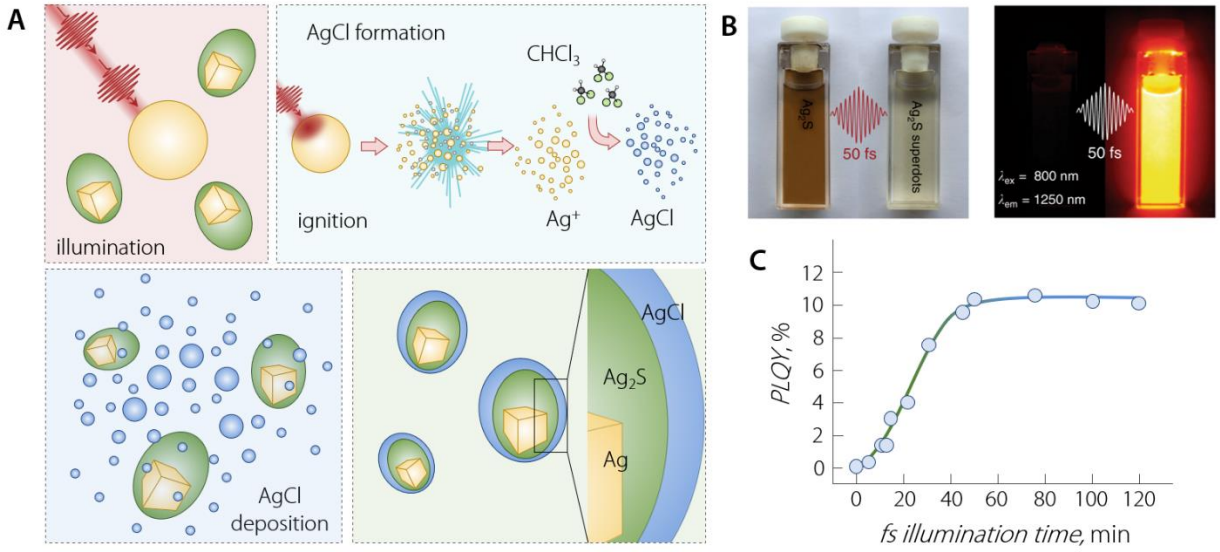

Figure 6. Preparation of Ag_2S/AgCl superdots. The formation of superdots is triggered by irradiation with NIR ultrafast laser pulses (A). This process entails a Coulomb explosion of Ag NPs present as byproducts, followed by reaction of the released Ag^+ ions with CH_3Cl to form AgCl, which ultimately

deposits on the surface of Ag_2S NPs forming a protective shell. The emission of the superdots is greatly brighter than the one of parent Ag_2S NPs under 800-nm excitation (B). The increase in PLQY before and after irradiation is 100-fold (C). Adapted with permission from xxxx.

QDs and RENPs have operation capabilities both in the visible and NIR, thus they are suitable for *in vitro* as well as *in vivo* use. On the other side of the spectrum, carbon-based materials such as CDs and CNTs are the NP of choice as far as lack of intrinsic compositional toxicity goes. Moreover, the production of this materials follows green(er) methods and there is little to no issue related with handling of the NP suspensions or solvents used during the synthesis. However, the emission of CDs cannot yet be satisfactorily in the BW-I/II range,[90-92] while NIR-emitting CNTs are generally not bright enough and their morphology is source of worry in terms of toxicological effects (*vide infra*).

All this being said, we argue that in the case of a single exposure to inorganic NPs for diagnostic purposes the drawbacks and risks for the patient associated with the intrinsic toxicity of elements composing the NPs could (on a general level) be overlooked. However, problems could arise in the study of chronic or slowly developing diseases that would require the acquisition of multiple images, i.e. the repeated administration of inorganic NPs. In this case, the concentration of NPs in those organs retaining them could overcome the damage limit. In pre-clinical units, the use of NPs containing hazardous elements could be instead justified, particularly for *ex vivo* or *in vitro* experiments aimed to investigate biological phenomena. However, a gradual farewell particularly from NPs containing heavy metals is both far-sighted and judicious. Firstly, it is foreseeable that restrictions on the use of those hazardous materials might be put in place in the (more or less far)

future. Secondly, the toxicological impact of materials containing heavy metals should be considered at different stages of the NP life cycle (production, handling, storage, and disposal). And in this perspective, the risks become higher, due to cumulative toxic effects and the possibility of these elements to enter the food chain.

4.1.2. Size and morphology. One of the main characteristics of NPs is their large surface-to-volume ratio. This geometrical consideration is pivotal since it translates to a higher surface available for interaction with the environment. The surface of a material – particularly at the nanoscale, where exceedingly small curvature radii are found – is substantially different from the bulk, featuring vacancies, dangling bonds, and strained lattice.[32, 93, 94] Thus, overall, the surface of NPs is disseminated with high-energy sites that are highly reactive. Moreover, the surface of QDs and RENPs is inherently positively charged, due to the presence of exposed metal ions with unsaturated valency.[95] These two last considerations carry less weigh in this frame though, and they become more relevant when designing surface functionalization strategies. Given the above, it is not surprising that often a trend has been observed that correlates smaller size of the particle to a higher toxicity,[96, 97] although this is not always the case and case-by-case distinctions should be made (**Figure 7**).[98]

The size of NPs has also an impact on the penetration capability through specific physical barriers. For instance, it was observed how smaller (20 nm) insulin-coated NPs more efficiently cross the blood brain barrier (BBB) than larger ones (50 and 70 nm).[99] Similarly, in another study, polysorbate-coated polybutylcyanoacrylate NPs with a size smaller than 100 nm were shown to trespass the BBB more effectively.[100] At a cellular level, Guo et al. showed that hydrophobic lipid-covered gold NPs show different kinetics in the translocation through a lipid bilayer.[101] In particular, NPs with a diameter below 5 nm remains trapped in the bilayer, while larger particles

can translocate through it. However, as discussed below, the crossing efficiency of NPs into specific tissues and cellular membranes is greatly influenced by the surface chemistry of the NPs, with the chances to accumulate in different brain regions being governed by the type of functionalization.[102, 103]

We should observe at this point that NPs in suspension might form aggregates. Due to geometrical factors, these aggregates can interact in a different way with cells compared to single NPs of equivalent overall volume.[104] Ideally, one would want a suspension to be administered where single NPs are individually dispersed and do not aggregate over time.[105, 106] This allows avoiding possible enhanced toxicity featured by aggregates, although there are contrasting reports regarding this increased toxicity.[104, 105] It also prevents the broadening of the size distribution of the NP ensemble, which can lead to different behaviors featured by populations of NPs with different sizes (see **Figure 3**). The colloidal stability and lack of unwanted aggregates in suspension is hence another relevant aspect. To that end, the strategies developed to impart biomimetic/biocompatible features to a NP (see **Section 4.1.2**) generally also afford long-term stability to the suspension. When a NP suspension is injected intravenously, the flow of the blood stream is expected to prevent aggregation between the NPs. So, aggregation is mainly investigated when the NPs reach a specific tissue. Indeed, sometimes controlled aggregation is harnessed to increase the effectiveness of the delivery at the desired site. For instance, pH-[107, 108] and MicroRNA-induced[109] aggregation of gold NPs has been used as a means to promote accumulation at solid tumors and retention within cancer cells.

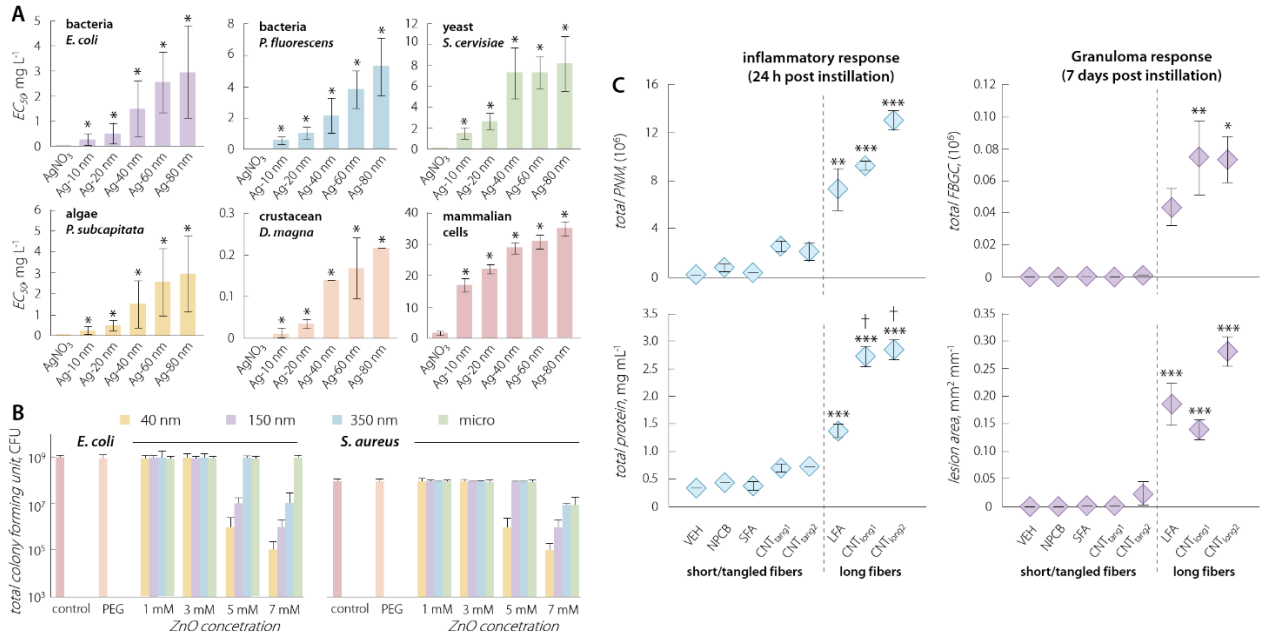

Figure 7. Dependence of toxicity on the size of NPs. 50% effective concentration (EC_{50}) values obtained after exposing different cellular lines (vegetal and animal) to silver NPs of different size (10, 20, 30, 40, 60, and 80 nm) compared to the effect of a solution of $AgNO_3$ (A).[96] Adapted with permission from xxxx. ZnO particles show a size- (and concentration-) dependent toxicity towards *E. coli* and *S. aureus*, with smaller NPs more sizably curbing the growth of the respective cell colonies (B).[110] Adapted with permission from xxxx. In the case of CNTs, longer fibers elicit a stronger inflammatory response and a larger number of granulomas in the mesothelial lining of the body cavity of mice, compared to shorter or tangled (i.e., effectively smaller and with a smaller aspect ratio) CNTs.[111] Adapted with permission from xxxx.

Size is not the only geometrical factor at play when gauging the toxicity of NPs. For instance, it is a well-established fact now that CNTs, despite their biocompatible chemical composition, have inflammatory and carcinogenic potential on par with the geometrically similar asbestos fibers (**Figure 7C**).[112] This behavior is a result of the extreme aspect ratio (length/diameter) of CNTs, as also proven by the fact that the toxicity scales with their length (from hundreds of nanometers to

few micrometers).[111, 113] It is to be noted that the toxicity of CNTs mainly arises from their inhalation followed by their nesting within the tissues of the lower respiratory tract.[114] This partially limits the concerns for their use in fluorescence imaging since dispersions are employed, thus averting the presence of airborne CNTs. Aside from this specific case, the NPs used in fluorescence imaging are generally much less anisotropic with a sphere-like morphology or, in general, low aspect ratios. Therefore, save for CNTs, this aspect is one of the least worrying as far as toxicity is concerned.

4.1.3. Surface chemistry. This parameter is by far the most important in determining the fate of a NP and its interaction with biological tissues – and as such its toxicity as well as its capability to target specific tissues.[102] The chief impact of surface chemistry over size and morphology has been showcased several times for different NPs: e.g., gold nanorods, RENPs, and QDs.[78, 115] For instance, heavy-metal-free InP QDs have been shown to exhibit cytotoxicity when featuring amine groups on their surface, while hydroxyl- and carboxyl-bearing QDs are not toxic.[116] This is a direct consequence of the presence of positively charged cationic species ($-NH_3^+$) as compared to negatively charged anionic ones ($-COO^-$). In general, a surface featuring positive charge is associated with higher cytotoxicity, due to its stronger interaction with the cellular membrane.[117] Surface charge is a key parameter also for the internalization of NPs by cells, along with size and morphology.[118] The step of internalization is fundamental to guarantee the residence of NPs at the site of interest, and it usually proceeds via two types of pathways: endocytosis-based uptake pathways and direct cellular entry. As mentioned in **Section 4.1.2**, induced aggregation can also be exploited to avoid exocytosis once the particles have been internalized via endocytosis.[109] Not only the pathway through which the internalization occurs depends on the NP parameters, but also

on the cell type. For a comprehensive summary of the state-of-the-art of cell uptake and trafficking, the reader is encouraged to read the recent review by Donahue et al.[118]

The subject of surface functionalization of NPs is incredibly broad, and it represents a consistent part of several review articles dedicated to the use of NPs for biomedical applications.[118-122] Simply put, a successful surface functionalization boils down to finding the right balance between minimizing interactions with biological components that elicit an immune response (and hence premature clearance of the NPs), while prompting selective recognition and interaction with cells that form the tissue of interest. Silica coating,[123-125] as well as the use of zwitterionic molecules[126, 127] or polymers[128] are amongst the most explored strategies to enhance biocompatibility and extend NP circulation time. Decoration with polyethylene glycol (PEG), in particular, is often regarded as the golden standard for imparting "stealth" properties to NPs.[129, 130] This approach builds on the success obtained with PEGylation of proteins in terms of improving the circulation time by preventing uptake from macrophages.[131] However, more studies have shown that PEG antibodies are produced upon repeated injections of PEGylated species.[132, 133] In fluorescence imaging, this translates to possible premature uptake of the PEGylated contrast agent, hence a shorter circulation time and less effective accumulation at the desired site.

But, even considering perfectly stealth NPs, how do we achieve their selective accumulation at the desired site? Countless are the examples in the literature of intratumoral injection of NP suspensions followed by imaging and/or treatment of the tumor.[134-136] Needless to say, these approaches are not applicable in the clinical practice and they can be justified only in proof-of-concept studies, where emphasis is put on the side of the material or an innovative treatment. The ideal scenario is to have a NP that can be injected intravenously in the proximity of the tissue of concern, and that autonomously identifies and accumulates in correspondence of the targeted

cells.[137] This can be achieved taking advantage of two approaches: passive and active targeting.[138, 139] The former approach is applicable when targeting solid tumors since it leverages the enhanced permeation and retention (EPR) effect: the natural extravasation of NPs in correspondence of tumoral tissues, where the blood vessels are defective (fenestrated). Nonetheless, a better selectivity is achieved by tethering targeting moieties to the surface of the NP. Folic acid, small peptides, antibodies, aptamers, and other biologically active molecules have all been used to target specific cells.[140, 141] The complementarity between the moieties attached to the NPs and cellular receptors is key to successful accumulation as well as internalization by the cells. To make things even more complicated, in some cases to reach a certain tissue some physical barriers have to be overcome. The most famous and difficult to cross is arguably the BBB, whose effectiveness in preventing non-specific crossing (and thus in protecting our brain) is the also the reason for the difficulty in accessing the brain with NPs through the circulatory system.[142] But brain is not the only organ/tissue that is difficult to reach. Indeed, great effort is being invested to improve the targeting efficiency of tumors after intravenous injection of NPs. The increasing number of publications focused on tumor targeting using NPs is testimony to this effort (**Figure 8**). Despite of this trend, the targeting efficiency (% of injected NPs reaching tumor site) unfortunately remains firmly below 1%. Therefore, future investigations devoted to modifying the pharmacokinetics of injected NPs to increase the targeting efficiency are desirable.

With all that being said, we believe that future research efforts for NP surface functionalization should be directed towards the personalization of nanomedicine.[143] One powerful approach is the use of membrane cells already present in the body,[144] thus relying on the naturally available product of millions of years of cellular evolution. For instance, using xenografts from patients, it has been shown that one can prepare cancer-cell-membrane-coated NPs for personalized cancer

treatment or tumor imaging (**Figure 9**).[145, 146] This approach exploits the tendency of tumor cells to adhere one to another, which can be harnessed to promote accumulation of coated NPs at the tumor site. Red blood cells and platelets can be used as sources of biomimetic membranes too,[147, 148] since they are recognized as endogenous components from the body, thus eliminating risks of NP opsonization and premature clearance.

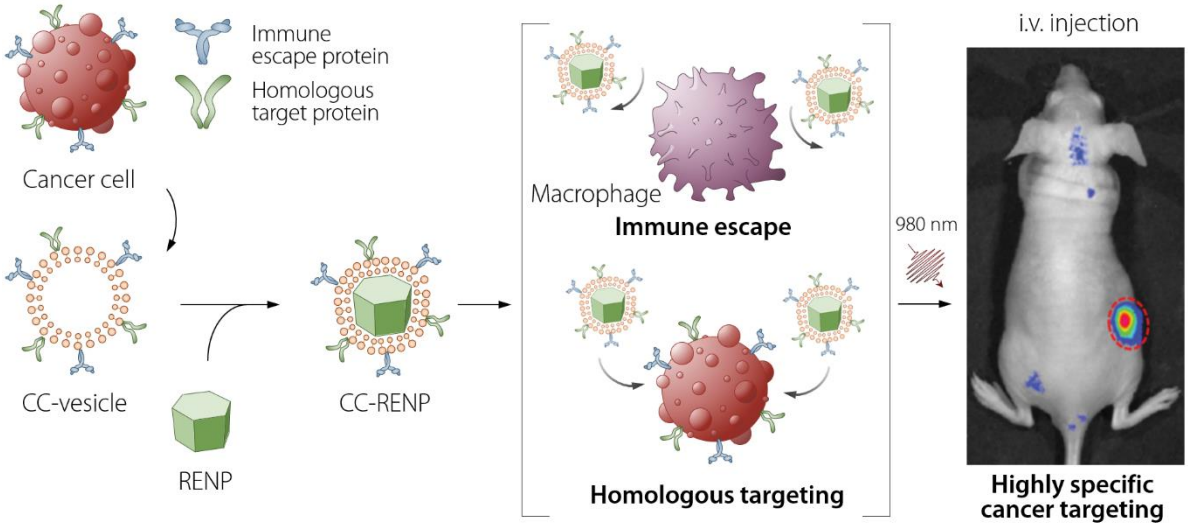

Figure 9. Scheme of the preparation, action and use of RENP coated cancer cell vesicle. The membrane of cancer cells can be used to prepare vesicle bearing membrane proteins. RENPs (in this case $NaYF_4:Yb^{3+},Er^{3+}$) can be encapsulated in this vesicle. The resulting vesicle-coated RENP exhibits immune escaping and homologous targeting capabilities inherited from the source cancer cells.[145] Adapted with permission from xxxx.

Further functionalization (either via surface conjugation or lipid insertion) can be performed to enhance selective targeting capabilities. Of course, any cell membrane can be used depending on the foreseen use of the NPs. This approach might allow also to avoid/limit the formation of a so-called *protein corona* (PC) atop of the NPs when they enter a bodily fluid (**Figure 10**).[149] This PC

is composed of proteins found in the body fluid, and its composition determines the fate of the NP, governing the interaction with biological species.[150] Indeed, even PEGylated nanoformulations approved for medical use gets covered by the PC, which has the fingerprint of the environment in which the NPs are introduced.[151] The use of molecules that are already present in the body to coat the NPs should minimize issues related with PC formation and changes in the NP surface chemistry induced by it. Customization of nanoformulations by harvesting these cells from the patient, the encapsulation of NPs within the extracted membranes, and further functionalization with (bio)molecules to enhance active targeting is expected to open the door to an ever more effective diagnosis and treatment of a number of diseases. For the specific case of luminescence imaging, this window of opportunities is in any case restricted by some physical considerations that are intrinsic of the imaging modality, as we discuss in the next Section.

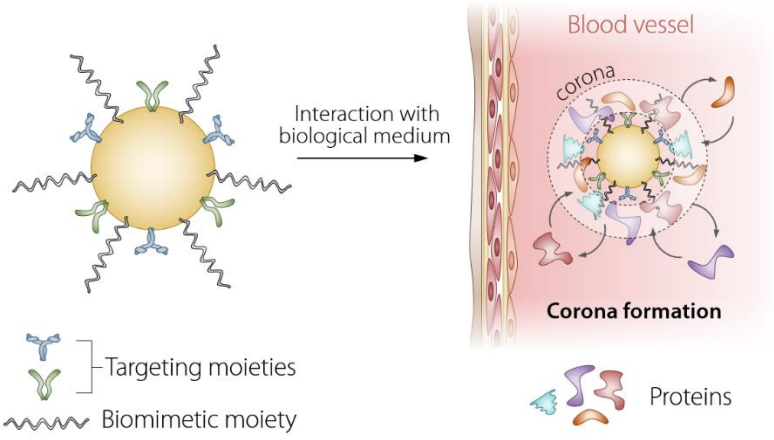

Figure 10. Protein corona formation. When a NP enters the body and gets in contact with a biological fluid, the proteins that are present in the fluid interact with the surface of the exogenous species. Different proteins have different affinities towards the surface of the nanoparticles. This differential affinity results in a composition of the protein corona that depends on the surface chemistry of the NP as well as the nature of the body fluid. Note that due to the adsorption of these proteins, the bioactive form of the NP

(i.e., bearing a protein corona) is *de* facto a different species from the one before the injection in the body, to the point of potentially compromising the targeting capabilities of the NP.

4.2 Brightness and tissue-induced attenuation: will we ever give the required attention?

In NP-based fluorescence imaging, the signal level is of paramount importance. Indeed, as of late we are witnessing an ever-increasing number of technologies being proposed, which aim at improving the contrast between the signal level and the autofluorescence present in biological tissues. Probably the most remarkable one entails the incorporation of time-dependent analysis of fluorescence images obtained under excitation with a pulsed source.[152-154] This strategy affords removal of the background contribution of autofluorescence (characteristic of biological tissues) and significantly improves the quality of the image. Nevertheless, even after applying this general optimization procedure, the tissue-induced attenuation of light and the low fluorescence efficiency of NPs are still drawbacks that are hard to circumvent under *in vivo* conditions. Thus, to expand the applicability of NP-based fluorescence imaging, a two-pronged action is necessary: (i) increase the fluorescent efficiency (fluorescence brightness, defined later) and (ii) minimize the effects of the optical extinction caused by tissues.

4.2.1. Looking for brighter NPs. The pursuit of evermore bright NPs is an ongoing process. . In fluorescence imaging, one of the main drives for this search is the fact that if brighter NPs are used, fewer of them are required for acquiring an image. This alleviates concerns related to the injection of a too large number of exogenous species in the body, with the possible adverse effects they might have. One of the most important parameters in the improvement of the fluorescence of

a given NP is the PLQY.[155] As previously indicated, PLQY (Φ) is defined as the ratio between the number of photons emitted and the number of photons absorbed.[156] Though researchers looking for high-brightness NPs often focus on increasing the PLQY, years of experience have shown that this strategy is insufficient, as a high PLQY coupled with low absorption efficiency of the excitation light also yields a poorly luminescent material. To account for the interplay between these two quantities, the concept of brightness (PLQY times the absorption coefficient) is introduced. It is especially useful when comparing different luminescent materials or probes.[156]

The strategies that must be followed towards the increment of brightness are clear: on one side, the development of highly absorptive NPs and, simultaneously, the modification of the NP structure to enhance the PLQY. The second half of this double approach implies the enhancement of radiative transition probabilities. In NPs, this is achieved by reducing surface defects that act as luminescence quenchers and an isolation of the NP from environment molecules whose vibrations promote nonradiative decays.[157, 158] The preparation of core/shell structures represent an optimal approach in this context. The presence of a protective shell has been already widely demonstrated to produce significant enhancements in the PLQY of luminescent NPs.[73, 159] The question now is to develop the required technology that would allow for the growth of a homogeneous and continuous shell enhancing, rather than frustrating, the optical properties of the core NP. Unfortunately, a one-size-fit-all solution does not exist. One example is the case of PbS QDs, whose PLQY cannot be effectively increase via ZnS shelling,[160] a strategy proven successful with most semiconductor NPs.[88, 161] In this sense, some of the authors of this Perspective recently demonstrated how combination of ultrafast photochemistry with traditional wet chemistry could lead to core/shell Ag_2S NPs with PLQY close to 10% (as illustrated in **Figure 6**).[32] This is a remarkable result, considering the usually low values of PLQY featured by Ag_2S NPs.[162]

Following this path, we believe that more unconventional yet effective strategies might and should be developed to push the boundaries of achievable PLQY.

On the other side, one can focus on the increase of the excitation light absorption capability of the NP. In this context, QDs have an edge on RENPs, with a light absorption cross section three to ten orders of magnitudes larger (σ_{QD} = 10^{-17}-10^{-11} cm^2 vs σ_{RE} = 10^{-21}-10^{-20} cm^2). CNTs have a larger absorption cross section compared to single RE^{3+} ions (σ_{CNT} = 10^{-18}-10^{-17} cm^2) too. No reliable data could be found for single-photon excitation of CDs, multiple-photon excitation processes being instead much better quantified in these NPs.[163] Given the poor absorption capabilities of RE^{3+} (owing to the forbidden *4f-4f* nature of most of the electronic transitions involved in the photoluminescence of these ions[164]), RENPs are the contrast agents that would more substantially benefit from a boost of their light harvesting prowess. To that end, coupling of semiconductor NPs and RE^{3+} has been performed both decorating RENPs with Ag_2S[165] or Ag_2Se[166] NPs, and doping RE^{3+} ions in QDs.[167] These strategies are incredibly advantageous on paper, but they involve the step of energy transfer from the absorbing moiety (semiconductor NP) to the emitting RE^{3+} ion: a critical step whose efficiency often limits the efficacy of these approaches. The use of plasmonic moieties coupled to luminescent NPs is another highly coveted strategy, which has been used in several occasions both for enhancing absorption and/or emission efficiency of RENPs[168] as well as QDs.[169] Harnessing the plasmonic effect is also challenging, as quenching instead of photoluminescence enhancement can be prompted if the relative position between plasmonic moiety and fluorescent NP is not precisely controlled.[170]

All in all, we believe that combination of strategies to increase the PLQY (i.e., *ad hoc* developed shelling procedure) and absorption (i.e., plasmon-induced improvement of absorption and/or

emission probability) could lead to brighter contrast agents whose use could push one step further the performance of fluorescence imaging.

4.2.2. Tissue attenuation. Even in the case of having at disposal the brightest possible NP to be used as contrast agent, the problem of low contrast of the images still poses a serious impediment. There are indeed further limitations that should be taken into consideration. Some of them could be overcome, others would simply have to be embraced by the scientific community. The latter is the case, for instance, of the conditions imposed on the irradiation dose.[171-174] More difficult to tackle is the issue of light attenuation in a biological system, as it is something entirely determined by the optical properties of the tissues (**Figure 11**).[175-177] Though the exploitation of biological windows (BWs) in the electromagnetic spectrum certainly minimizes these problems,[10, 178, 179] the strategy does not completely extinguish it. For the sake of illustrating the implications of these restrictions, let us consider an idealized luminescent NP with a quantum energy efficiency (defined as the ratio between the energy output and the energy input)[156] of 100%. Even in the situation where this material is found underneath a layer of one of the most transparent human tissues in the BWs (grey matter, for instance[180]), both the excitation and emission light are still absorbed and scattered. For our purposes, let us also consider the use of a BW-I excitation source, as it has been proven to minimize undesired heating effects,[29, 30, 181] and that the emission is found in BW-II. Considering that the more external part of the grey matter has a usual thickness of 10 mm and average attenuation coefficients of 0.07 mm^{-1} and 0.06 mm^{-1} in BW-I and BW-II, respectively, this means that 50% of the excitation light does not reach the NP and that 45% of the subsequently generated emission is not transmitted to the detection system. Compared to the case where the sample is directly illuminated by the laser, this means a total loss of 73% of the intended emission. Such a value, however, might still be acceptable for biomedical applications. Had another tissue

been chosen, the total loss would be even higher. The skin, for instance, has average attenuation coefficients of 16.0 mm^{-1} and 16.6 mm^{-1} in BW-I and BW-II, and would provide a total loss of more than 90%.[17, 182] The situation, of course, is worsened in real-life scenarios where a composite tissue is found before the material – beside the fact that NPs used as contrast agent have quantum energy efficiency below 100%.

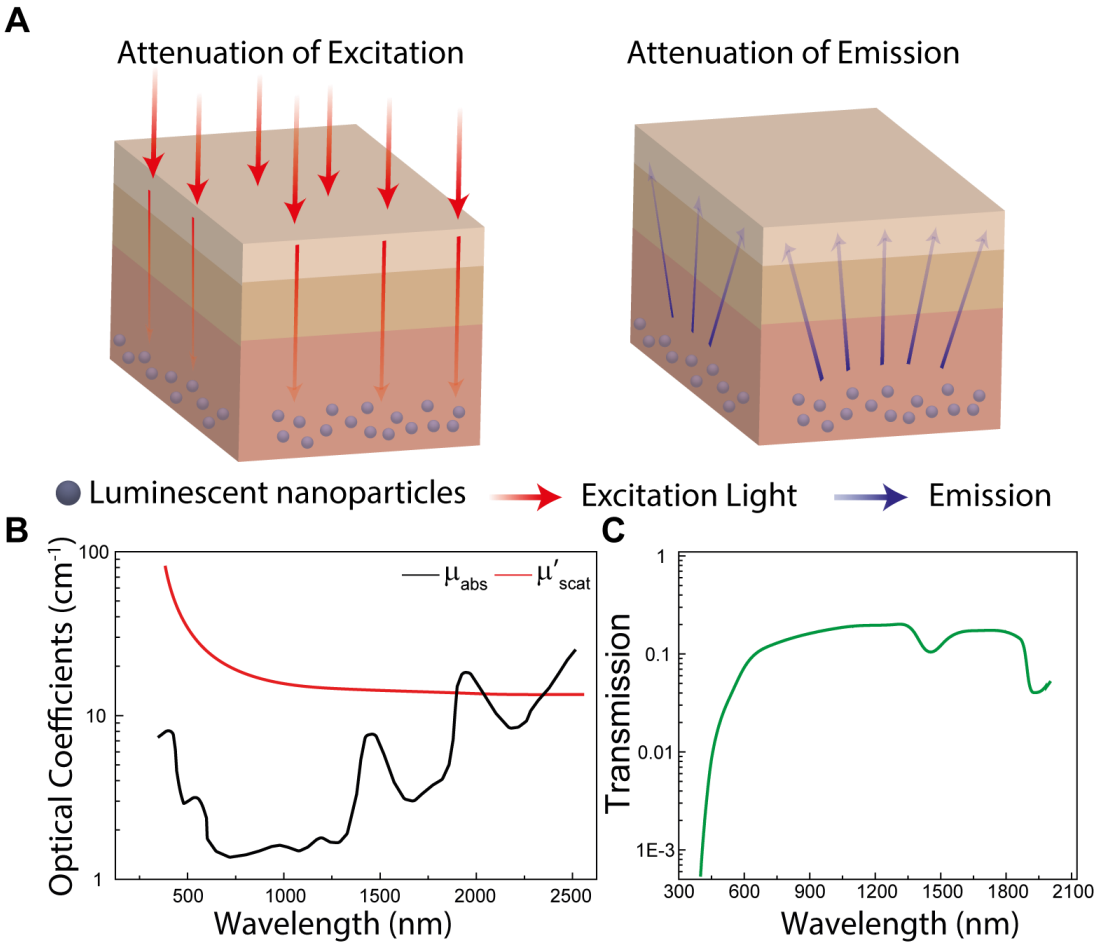

Figure 11. Effects of light attenuation in biological tissues. Simplified depiction of the transmission of excitation (left) and emission (right) through biological tissues (A). Wavelength dependence of the absorption and reduced scattering coefficients of human skin in the visible and NIR (B).[182] Percentage of light that successfully passes through 1 mm of human skin as a function of the wavelength (C).

4.2.3. Pathways to address the "tissue attenuation" issue. To overcome these large attenuations, one could try any of these two solutions: (i) increase the excitation power so that more excitation photons reach the contrast agent, causing more photons to be emitted and, therefore, detected, or (ii) increase the exposure time so that more signal is collected. While the first approach can prove to be useful in fields such as fluidics and electronics, it is not viable when dealing with biological tissues. Because certain safety guidelines need to be followed, the irradiation dose must never surpass a well-established maximum value.[171-174] Despite some internal disagreements in the literature, a maximum excitation power density of 330 mW/cm^2 is generally accepted for the study of tissues under normal conditions.[171, 183] If a photothermal treatment is being induced, however, this maximum value could reach up to 2 W/cm^2.[184] Be that as it may, increasing the excitation power is neither a safe nor a universal approach. On the other hand, increasing the exposure time does not necessarily compromise the health status of the tissue if the irradiation dose is found within the safety limits. Notwithstanding, it generates problems of other nature. The most obvious ones being the loss in temporal resolution and accumulative heating during illumination. Furthermore, the effectiveness of the approach might also be compromised by the technological limits of the detection systems. Case in point, even after increasing the exposure time, if the transmitted intensity is only slightly higher than the noise-equivalent irradiance (NEI, i.e. is the flux density that results in a signal-to-noise ratio of 1) of the camera, the detected signal will be too poor for an accurate analysis.

Since these problems are mainly imposed by the optical properties of the various biological tissues, their corresponding solutions can only be resolved if one tries first to determine the best possible outcomes when dealing with different organs. Only then, the expectations can start to be realistic. To illustrate this concept, the potential of narrowband NIR-emitting NPs for applications in various

human organs was evaluated. For the sake of brevity, we chose a model NP that can be excited in BW-I and that emits in BW-II. This, as mentioned several times throughout this Perspective, is a very common situation.[26, 185-187] For each case studied, the NPs were considered to have preferential accumulation in a specific organ. The optical properties of this organ, in turn, were registered (according to literature) alongside with the ones from the surrounding tissues. By taking into account their average thicknesses in an adult, it was possible to determine, in a first approximation, (i) the fraction of excitation light that gets into the organ I_{exc}^{del}/I_{exc}, and (ii) the fraction of emitted light that gets detected, I_{det}/I_{em}. The main results are included in **Table 2** and they reveal that, even if the luminescent NPs could accumulate in any desired human organ, most measurements would still result problematic. After all, many organs provide values of I_{det}/I_{em} and I_{exc}^{del}/I_{exc} below 10^{-8}%. This means that, depending on the excitation energy initially delivered, the emitted light might not be detected at all. Thus, to verify which cases could result in viable applications, we considered, without loss of generality, the excitation irradiance to be κ_{exc} = 330 mW/cm^2 (i.e. the allowed maximum[171]). Under such conditions, the maximum detected irradiance, k_{det}^{max}, is obtained through:

$$\kappa_{det}^{max} = \kappa_{exc} \left(\frac{I_{exc}^{del}}{I_{exc}}\right) \eta \left(\frac{I_{det}}{I_{em}}\right) \qquad \text{Eq. 1}$$

where η is the quantum energy efficiency of the NPs. If one, once again, considers the best-case scenario where η is equal to 100% (maximum imposed by energy conservation), one then finds the data included in the rightmost column of **Table 2**. By taking into account that the noise-equivalent irradiance (at 1s of exposure time) of InGaAs cameras currently available in the market is of the order 10^{-12} W/cm^2,[188] then the straightforward conclusion is that the NP luminescence

could only be detected in a small set of human organs. In fact, broadly speaking, **Table 2** presents at least four different situations:

- **Optimal.** k_{det}^{max} always exceeds the order of 10^{-12} W/cm^2. The organs that satisfy this condition are highlighted in green in the last column. If luminescent NPs are located within these organs, their light is very likely to be detected.
- **Circumstantially positive.** k_{det}^{max} is circumstantially higher than 10^{-12} W/cm^2 (highlighted in blue). This is the case, for instance, of bones. After all, depending on which bone one selects, there might be certain muscles around it and, consequently, more attenuation. Other bones (such as the ones in hands and feet) might be less affected by attenuation.
- **Potentially positive.** The case of those organs whose k_{det}^{max} were found between 10^{-18} W/cm^2 and 10^{-12} W/cm^2 (i.e., lower than NEI but only by a few orders of magnitude). Though certainly below the detection limits, the possibility of detecting light coming from these organs could have been negatively affected by the first-order nature of the approximation. This is important to consider because a simple Beer-Lambert law analysis cannot account for the role of the geometry of the tissue and, for instance, the non-additivity of the scattering effect. Furthermore, there is no consensus on their optical coefficients (differences of up to 40% in the mean value have been reported in different works in the literature).[189-195] These facts, together with the possibility of increasing the exposure time or the excitation irradiance (photothermal therapy), could actually result in light being detected. Therefore, by recognizing the limits of our approximations and the accuracy of the data provided in literature, we were led to

classify these as potential candidates to be imaged via NP-enabled fluorescence imaging. They are highlighted in orange.

- **Negative.** The case where the application of luminescent NPs is not viable even after considering the discrepancies in literature over their optical properties and the simplified nature of the approximations. In terms of k_{det}^{max}, these were the organs which had a maximum detected irradiance below 10^{-18} W/cm^2. To justify such a value, one only needs to think about the worst-case scenario where (i) the Beer-Lambert Law, (ii) the discrepancy on the optical coefficients and (iii) the low integration time (or low excitation irradiance) is each one reducing the value of k_{det}^{max} by two orders of magnitude. If that were the case, k_{det}^{max} would still fall behind 10^{-12} W/cm^2. Such organs are highlighted in red.

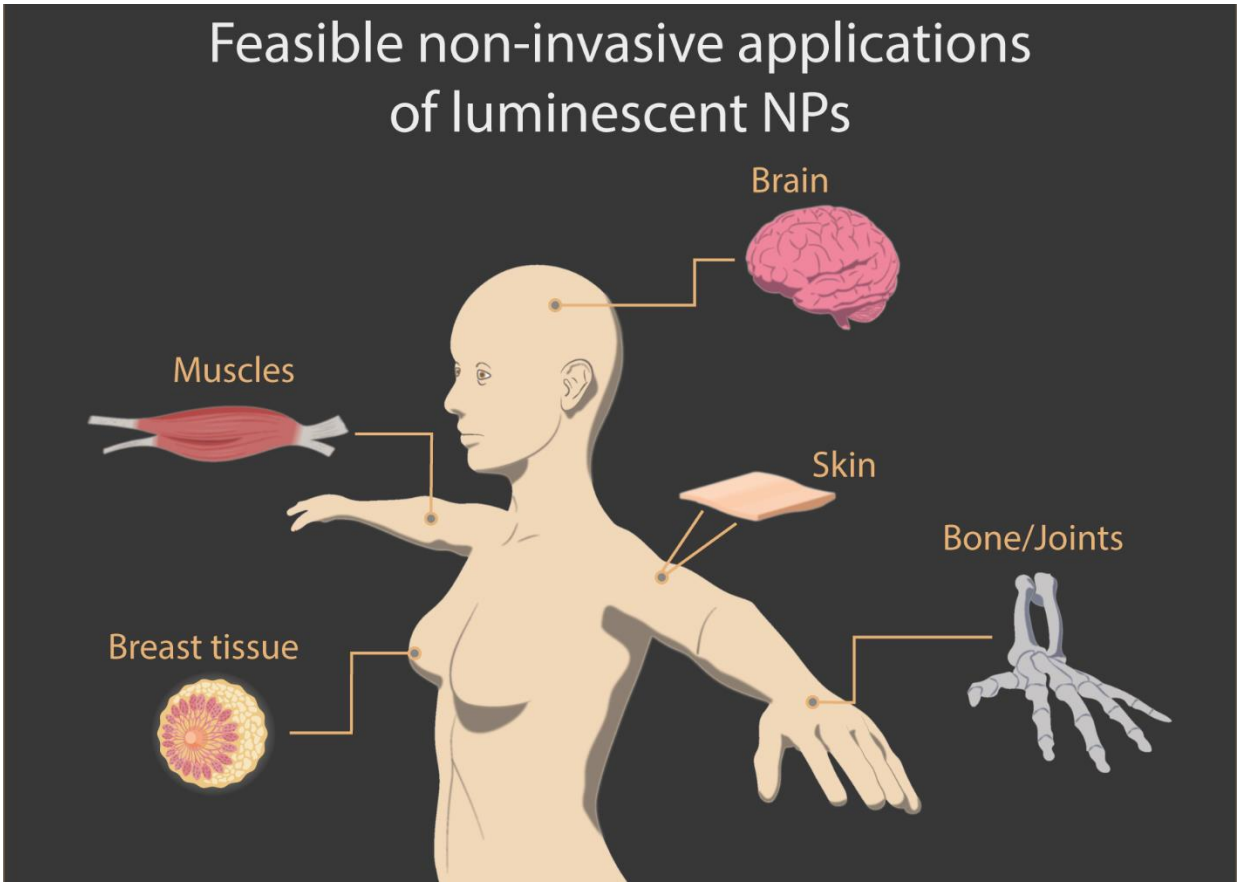

Figure 12. Feasible non-invasive applications of fluorescence imaging through luminescent nanoparticles. Main human tissues identified as optimal (or at least possible) for investigation with NP-based fluorescence imaging after considering the limitations imposed by the scattering and absorption of NIR light in biological tissues. The identification was based on the data inserted in **Table 2**.

Thus, a careful look into **Table 2** suggests that, if the optical coefficients reported in the literature are to be trusted, luminescent NPs and fluorescence imaging can only be feasibly applied in five main human tissues: skin, bones, muscles, breast, and the outer part of the brain (**Figure 12**). This conclusion is certainly more modest than what most of the works dealing with *in vivo* applications of luminescent NPs in animal models tend to suggest. The reason why these studies overestimate the potential for human applications is primarily related to the reduced dimensions of the animal under investigation. If one inserts the NPs into the liver of mice, an organ which for humans is

outside the detection range, the maximum detected irradiance is of the order of 10^{-4} W/cm^2 (assuming similar values for the attenuation coefficients and the dimensions of tissues provided in literature[196-198]) under 330-mW/cm^2 excitation. Such a value is way above the lower detection limit of currently available cameras. Thus, the community needs to be careful not to extrapolate their goals from animal models to humans when writing the studies.

Nevertheless, even if the expectations are lowered, one should not disregard the efforts that were put into luminescence-based nanotechnology in the last decades. After all, luminescent NPs can still play their role in the non-invasive detection and treatment of several malfunctions of the human body. This would include burdensome diseases such as osteoporosis, vitiligo, multiple sclerosis, stroke, breast cancer, and many others. Furthermore, the already established application at the small-animal level would also be beneficial from the point of view of better understanding the biological processes that take place during malfunctions of the body. The future of the field, therefore, is still promising. Interestingly enough, the five human tissues that were selected (**Table 1**) form the same set of tissues that are successfully studied in a well-established technique known as Diffuse Optical Tomography (DOT).[199-208] DOT is an ongoing imaging modality in which a tissue is illuminated by NIR light from an array of sources. Under such conditions, the scattered light which emerges from the tissue is observed with an array of detectors, and then a model of light propagation is used to infer the optical properties of the illuminated tissue. Following the reasoning so far proposed, the similarity in the applicability of fluorescence imaging and DOT is straightforwardly understood: both techniques are limited by the level of tissue-induced attenuation. By itself, this should already make the researchers more attentive to the possible overlap between the two techniques as well as their relative advantages and disadvantages. Luckily, a positive change of goals and expectations could result from that.

Though the non-invasive use of luminescent NPs in adult humans is clearly limited to some tissues, we are more optimistic when it comes to infants and children. After all, due to the reduced dimensions of their tissues, the number of organs considered as viable in **Table 2** would certainly increase. This, in turn, would open more possibilities for the detection and treatment of diseases. Such a concept, in fact, has already been explored in DOT for the deep-brain studies in new-born babies.[200, 209] Considering all the extra quality checks that will need to be fulfilled for the use in new-born, if luminescence-based nanotechnology follows a similar path, then the development of the materials should start focusing on these quality checks at the level of material design. Furthermore, the community will need to be ethically wise to consider the possible impediments that might arise. If, on the other hand, the intention is still to keep the applicability of luminescent NPs as broad as possible (including adults), then the use of endoscopic techniques will certainly have to be considered. In other words, if an endoscope is found in the proximities of the tissue of interest, the light coming from there can still be collected. Under these circumstances, however, the non-invasiveness can no longer be considered as one of the most attractive features of luminescent NPs.

Tissue	$<\mu'_{scat}>$ (cm^{-1})	$<\mu_{abs}>$ (cm^{-1})	Surrounding Tissues	$\frac{I_{det}}{I_{em}}$ (%)	$\frac{I_{exc}^{del}}{I_{exc}}$ (%)	κ_{det}^{max} (W/cm^2)
Skin[17, 182] (1.5 mm)	BW-I: 15.6 BW-II: 16.3	BW-I: 0.38 BW-II: 0.34	--	8.2	9.0	2.4×10^{-3}
Adipose tissue[182] (7 mm)	BW-I: 11.2 BW-II: 8.68	BW-I: 1.08 BW-II: 1.00	Skin (1.5 mm)	2.8×10^{-3}	1.3×10^{-3}	1.2×10^{-10}
Muscles[182] (10-30 mm)	BW-I: 5.95	BW-I: 0.46	Skin (1.5 mm), adipose tissue (7 mm)	8.1×10^{-7} - 8.3×10^{-4}	1.1×10^{-7} - 8.8×10^{-4}	2.9×10^{-18} -

	BW-II: 5.73	BW-II: 0.51				2.4×10^{-11}
Skull[210] (6 mm)	BW-I: 20 BW-II: 16	BW-I: 0.1 BW-II: 0.5	Skin (1.5 mm), possibly facial muscles (15 mm)	5.0×10^{-6} - 6.0×10^{-2}	1.5×10^{-6} - 2.2×10^{-2}	2.4×10^{-16} - 4.3×10^{-8}
Chest wall[211] (14 mm)	BW-I: 46.1 BW-II: --	BW-I: 1.29 BW-II: --	Skin (1.5 mm), adipose tissue (7 mm)	6.3×10^{-12}	6.6×10^{-18}	1.37×10^{-33}
Bone[16, 212, 213] (up to 25 mm)	BW-I: 16 BW-II: 10.5	BW-I: 0.02 BW-II: 0.07	Skin (1.5 mm), adipose tissue (7 mm), possibly muscle (up to 30 mm)	3.1×10^{-14} - 1.3×10^{-1}	6.8×10^{-21} - 2.2×10^{-2}	6.9×10^{-39} – 9.4×10^{-8}
Dura mater[214] (2.5 mm)	BW-I: 8.27 BW-II: 9.52	BW-I: 0.5 BW-II: --	Skin (1.5 mm), Skull (6 mm)	1.8×10^{-5}	1.2×10^{-4}	7.2×10^{-14}
Breast[215] (up to 55 mm)	BW-I: 12.0 BW-II: 10.0	BW-I: 0.13 BW-II: 0.20	Skin (1.5 mm), adipose tissue (7 mm)	2.1×10^{-9} - 3.5×10^{-7}	2.1×10^{-11} - 9.0×10^{-7}	1.4×10^{-24} – 1.0×10^{-17}
Parietal Peritoneum[216] (14 mm)	BW-I: 11.0 BW-II: 11.0	BW-I: 12.0 BW-II: 10.0	Skin (1.5 mm), adipose tissue (7 mm), muscle (5.6 mm)	6.7×10^{-5}	1.8×10^{-5}	4.0×10^{-14}
Stomach[217] (46 mm)	BW-I: 7.59 BW-II: 7.62	BW-I: 1.0 BW-II: 2.5	Skin (1.5 mm), adipose tissue (15 mm), muscle (5.6 cm), parietal peritoneum (1.4 mm)	9.6×10^{-18} - 2.9×10^{-12}	6.6×10^{-18} - 1.5×10^{-13}	2.1×10^{-39} – 1.4×10^{-29}
Liver[218] (69.6 mm)	BW-I: 9.0 BW-II: 7.68	BW-I: 1.0 BW-II: 0.5	Skin (1.5 mm), adipose tissue (15 mm), muscle (5.6 mm), parietal peritoneum (1.4 mm)	4.6×10^{-20} – 2.7×10^{-14}	1.6×10^{-24} - 4.5×10^{-17}	2.4×10^{-48} – 4.0×10^{-35}

Lung[219] (102 mm)	BW-I: 20 BW-II: --	BW-I: 0.01 BW-II: --	Skin (1.5 mm), adipose tissue (7 mm), chest wall (14 mm)	2.4×10^{-54} – 7.9×10^{-16}	9.1×10^{-76}- 7.0×10^{-21}	7.2×10^{-134} – 1.8×10^{-40}
Intestine[214] (73.3 mm)	BW-I: 9.66 BW-II: 8.56	BW-I: 1.5 BW-II: 2.3	Skin (1.5 mm), adipose tissue (15 mm), muscle (3 mm), parietal peritoneum (1.4 mm)	9.9×10^{-11} - 6.5×10^{-9}	1.1×10^{-11} - 9.9×10^{-11}	3.6×10^{-26} – 2.1×10^{-23}
Brain (grey matter)[180] (10 mm)	BW-I: 0.7 BW-II: 0.6	BW-I: 0.02 BW-II: 0.04	Skin (15 mm), skull (6 mm), dura Mater (2.5 mm)	2.6×10^{-5} - 3.6×10^{-5}	4.1×10^{-6} - 5.8×10^{-6}	3.5×10^{-15} – 6.9×10^{-15}
Brain (white matter)[180] (15 mm)	BW-I: 5.2 BW-II: 3.0	BW-I: 0.08 BW-II: 1.00	Skin (15 mm), skull (6 mm), dura mater (2.5 mm), grey matter (up to 29 mm)	1.8×10^{-7} - 3.7×10^{-7}	1.4×10^{-8} - 5.5×10^{-8}	8.3×10^{-20} – 6.7×10^{-19}
Maxillary sinus[214] (15 mm)	BW-I: 6.07 BW-II: 4.79	BW-I: 1.00 BW-II: 1.00	skin (15 mm), skull (6 mm)	5.4×10^{-6} - 7.2×10^{-5}	3.7×10^{-7} - 6.3×10^{-6}	6.6×10^{-17} – 1.5×10^{-14}

Table 2. Potential of luminescent nanoparticles for non-invasive applications in human tissues. Estimation of the emitted light that gets to be detected (4th column), the excitation light that reaches the inner part of the tissue (5th column), the detected power density after considering an excitation irradiance of 330 mW/cm^2 and luminescent NPs with perfect quantum energy efficiency (6th column). In the more internal organs, the NPs were considered to be located between the center of the organ and the proximities of its surface. This, alongside the circumstantial conditions, contributed to defining the ranges of values in columns 4, 5 and 6. Dimensions were estimated with cryosections of the human body as provided by *The Visible Human Project*[220, 221]

Raising the stakes: fluorescence imaging and machine learning.

After laying out the problems related to the intrinsic limitations of fluorescence imaging imposed by the properties of luminescent NPs, tissue properties, and measurement setups, let us now delve into how artificial intelligence can provide a helping hand in this framework.

If we consider the use of fluorescence imaging in pre-clinical units, in addition to the problem of strong tissue-induced attenuation described in the previous section, the acquisition of fluorescence images requires complete immobilization of the animal under study. Typical integration times used for the acquisition of high-contrast *in vivo* fluorescence images are in the 0.1-1 s range. During this acquisition time the displacement of a free mouse could be as large as 1 cm. This causes the appearance of a relevant blurring in the acquired image. Traditionally this has been solved by immobilizing the animal under study, most of the times by applying anesthesia. This approach not only avoids blurring, but it also allows to use longer integration times and, in this way, the signal-to-background ratio in the fluorescence images is improved. However, depending on the goal of the imaging procedure, using anesthesia or physical constraints can be far from the ideal situation. For example, anesthesia is known to alter vital functions,[222, 223] and several works have reported on a general decrease of the metabolic activity and whole-body temperature during anesthesia procedures. Thus, readouts regarding vital parameters extracted from the analysis of fluorescence images taken on an anesthetized animal could be misleading or erroneous, since the system under investigation is altered by the measurement procedure. This could be especially relevant when imaging organs that have been demonstrated to be more heavily affected by anesthesia, like brain.[223-225] To overcome this limitation, imaging of freely moving animals becomes imperative.

Indeed, the need for imaging freely moving animals has motivated the community to upgrade traditional techniques. For instance, less than one year ago, Kyme and co-workers developed an experimental setup capable of acquiring PET images in "freely" moving, awake rats.[226] The experimental system (**Figure 13**) consisted of unmodified small animal PET system, a robot-controlled animal enclosure and an optical motion-tracking device.[226] Using this system, the authors were capable of imaging the impact of drug (amphetamine) administration on brain activity without the need for immobilization. Despite the important results obtained, the system still imposed severe motion restrictions to the animal (owing to the reduced space). Space restrictions limits the potential of this approach to one-animal studies and scotches the possibility of studying the impact that social interactions have on the vital function. Nonetheless, this study shows the way and demonstrates that the community is becoming aware of the importance of moving away from anesthesia to obtain results that paint a more truthful picture.

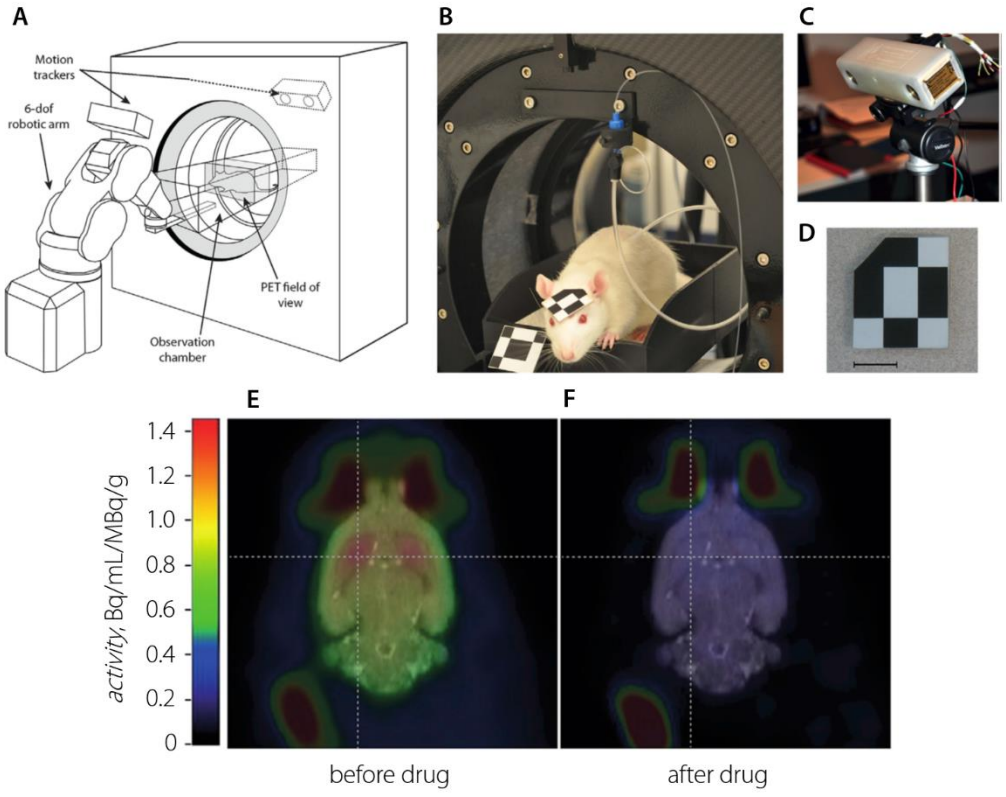

Figure 13. Acquisition of PET images in awake animal models. Kyme et al. a system for the acquisition of PET images in a moving animal (A) located in an enclosure (B) and whose motion is tracked with the use of a pair of CCD cameras (C) that can detect the accurate position of three rigid markers (D), one of them attached to the head of the animal and the other two at fixed positions. Motion-corrected PET images of the brain were obtained 20 min before (E) and 20 min after (F) drug (amphetamine) administration by following the displacement of [11C]raclopride by unlabeled raclopride.[226] PET images in E and F are superimposed to MRI images. Adapted with permission from xxxx.

The acquisition of fluorescence images of freely moving animals is clearly a challenging task. Because of the use of excitation laser sources and of fluorescence cameras, fluorescence imaging of freely moving animals implies to overcome two main technical limitations. Firstly, the technology making possible the localization of the animal within the experimentation cage should be incorporated in the imaging system. Secondly, a new procedure becomes essential for imaging acquisition and analysis to correct the blurring due to the rapid movements of the animal. This latter point requires knowledge of the animal position as well as prediction of its motion. These two requirements can be simultaneously satisfied using AI. To that end, deep learning has been recently applied for real-time tracking and motion prediction of freely moving animals.[227]

We anticipate that in the near future these algorithms could be implemented in fluorescence imaging systems already working in preclinical units. Knowing the exact location of the animal is necessary not only for determining the imaging field-of-view but also for selective and accurate excitation of contrast agents within the animal. This would be accomplished with the use of advanced optomechanics that, guided by the output of deep-learning algorithms, could direct the excitation light inside the experimentation cage with high spatiotemporal precision. In this scheme, AI could also be used to develop a module capable of combining information about animal position and motion together with the acquired fluorescence images, so to correct for image blurring. We

foresee that the implementation of AI-based technologies in this field could take some time, but we are convinced that the future of fluorescence imaging in preclinical units will be experimentation of freely moving animals.

Lastly, a point has to be made regarding spatial resolution, which is relevant both in the pre-clinical and in foreseeable clinical applications. As pointed out already in **Table 2**, the spatial resolution is primarily dependent on the scattering of the light emitted by the contrast agent at a specific depth within the tissue. Due to difference in optical properties, not all the tissues would afford the same spatial resolution in fluorescence imaging. To mitigate this issue, the use of AI could also prove advantageous since it is very efficient not only in image processing but also in solution of partial differential equation (PDE)-related problems (such as the propagation of light).[228] Indeed, convolutional neural networks (CNNs) have been successfully applied in computed tomography,[229-231] MRI[232-234] and more recently in DOT.[235, 236] When it comes to fluorescence imaging, this technique could train neural networks to reverse the problem of non-linear photon scattering and, as a consequence, reconstruct the original fluorescence signal coming from the NPs before being transmitted through the different set of tissues.[235] Such an application could extend the applicability of the field and even offer information on the possible anomalies present in organs/tissues.

Perspective and outlook.

Forthcoming development of fluorescent NPs for in vivo fluorescence imaging is greatly depending on how very specific aspects of such materials are going to continue being upgraded in the immediate future. All ofthree pivotal lines of action: below are in fact :

- ***Specific standards*** being developed, set and accepted community-wide, valid for a number of nanoparticles characteristic features, as they has been already analyzed and discussed in Section 4.1 above (*brightness*; *specificity*; and *toxicity*). That way, research community will be able to rigorously and quantitatively compare the new generation of fluorescent nanoparticles among them. Those standards should allow to rank the fluorescent nanoparticles not only depending on their intrinsic characteristics, but also weighing the use of such contrast agents for each specific tissue, as remarked through the Section 4.2.3, and in **Table 2** in detail.
- ***Reproducibility*** it is indeed an aspect very much related to the previous one, as such aforementioned NP features should nor differ from batch to batch. Tof the same class of nanoparticles neither critically depend heir performance not on *who* or–once the synthesis protocol officially consolidated. In the search of reproducibility , and the use of machine learning [237, 238]
- ***Functionalization***, as non-toxic, highly bright nanoparticles, emitting signal within the carefully chosen spectral range, are worth nothing if they don´t reach and the desired organ, or they don´t remain for time enough at such site.tissue . This requires advanced surface functionalization that should be accompanied by a complete understanding on how a nanoparticle interacts with cells and tissues at the in vivo level. In vitro experiments have resulted too optimistic when evaluating the targeting efficiency of functionalized nanoparticles. .

Ooutlook over the realistic chances ahead, for the broad use of fluorescent nanoparticles for in vivo imaging should be split, hence tackling two very different contexts: small animal imaging for research purposes (preclinical) both from applied and fundamental viewpoints; and

applications of fluorescence imaging in humans (clinical) for disease detection facilitating diagnosis or image-assisted therapies.

At the ***preclinical*** level, nanoparticle-enabled in vivo fluorescence imaging it is already a blooming reality in the imaging facilities of research institutions all around the globe. However, there are yet two steps to walk forwarplace fluorescence imaging at the same level as in PET, MRI, PA and CT ones. Analyzing the fluorescent nanoparticles specifically as contrast agents for in vivo imaging, they are arguably considered one echelon below small organic (fluorescent) molecules –this . not happening everywhere, but a widely enough conviction to deserve mentioning it. For the forthcoming generation of fluorescent nanoparticles to beat such competitor, or tie with it at least, further progress in terms of brightness of the nanoparticles, certainty about lack of toxicity, and clearance of the nanoparticles -once they have been used -are still required. In the positive side, fluorescent nanoparticles overpower small molecules in terms ofthree *emission tunability* (successfully shifting towards BW-II/BW-III emission); *narrow emission, and a large Stokes shift* (most of the nanoparticles); and*long photoluminescence lifetimes*. To be accurateThis last enable the use of counterpart, and that brings on the table the advantageous implementation of ttime-gate detection for reducing autofluorescence.

On the other hand, fluorescence in vivo imaging itself (preclinical), irrespective of the chosen contrast agent, has still pending to fully exploit, for preclinical applications. For instance, the best of what fluorescence imaging has to offer in terms of real-time monitoring (of metabolic processes, for instance) is yet to come. Moreoverbased on the continuousof infrared emitting of As an overall evaluation from a technical viewpoint, we must consider that whole body 3D fluorescence imaging of small animals is currently at hand within the next decade, counting on keeping the current rate

of two-pronged development of both fluorescent nanoparticles quality and BW-II/BW-III detection systems capabilities.

The ***clinical*** challenge deems a bit more elaborated perspective to be drawn, as it is a much more complex and multifaceted scenario. In the discussion below, we mostly cite works related to quantum dots/semiconductors nanocrystals as examples of the proven applicability of NP-enabled fluorescence imaging. That is not to imply that other fluorescent nanoparticles could not pass the bar for clinical applications anytime soon, but research in those semiconductor-based nanomaterials is now providing the most promising results.

we via so that itworking on the optimization ofon the development of better and cheaper on the incorporation of

As we mentioned in Section 4.2, the physical constraints regarding the applicability of fluorescence imaging in humans get relaxed in infants, owing to the intrinsic reduced size of organs and tissues. However, this is compensated by more stringent requirements to be met from the safety viewpoint., partially,Nowadays, the approved clinical use of fluorescence imaging is mainly limited to endoscopic and surgery-related applications. About the latter battleground, that imaging technique is deployed for real-time imaging of tumoral areas while surgery operations are taking place. Hence, it is of paramount relevance important to increase the certainty about avoiding unnecessary tissue removal. Moreover, that image-based monitored should guarantee that the tumoral mass be completely removed and thus averting resurgence. In that context, fluorescence imaging provides both high sensitivity and remarkable resolution (1 μm), but is hampered by the non-ideal properties of phosphors currently approved for oncologic indications like nonspecific tissue distribution, lack of stability, rapid clearance, and excitation and emission at wavelengths

that do not transmit deep enough inside tissues. The three fluorescent dyes currently approved by the FDA for cancer imaging are 5-aminolevulinic acid (5-ALA, fluorescence guided surgery), methylene blue (Sentinel Lymph Node –SLN- mapping), and indocyanine green (intraoperative tumor identification).[239-241] 5-ALA is approved for fluorescence-guided surgery, but is excited and emits at wavelengths (405/645 nm) that are heavily absorbed by tissue, which severely hinders imaging depth. Methylene blue is approved for SLN mapping and has more appropriate excitation and emission peaks (668/688 nm), but cannot be used at high doses due to the potential for toxic metabolic encephalopathy, is cleared quickly from tissue, and exhibits a small Stokes shift with largely overlapping spectra, making it difficult to differentiate between reflected excitation light and emitted light. [S. S. Kartha et al. Otolaryngol. Head Neck Surg. 2006, 135,765.; (b) S. B. Mondal et al. Adv. Cancer Res. 2014, 124, 171; (c) U. Resch-Genger et al. Nat. Methods 2008, 5, 763; (d) S. Q. Feng et al Biomaterials 2016, 103, 256.] As a result, methylene blue is typically used for its visibly intense blue color and not for fluorescence imaging. Indocyanine green also has fairly favourable excitation and emission peaks (807/822 nm), but has poor thermal and photostability, a small Stokes shift, and low photoluminescence quantum yield (PL QY) leading to low imaging contrast.[U. Resch-Genger et al. Nat. Methods 2008, 5, 763; (b) S. Q. Feng et al Biomaterials 2016, 103, 256.]] In addition, because all three are small molecule dyes, they are cleared quickly by the lymph system.[242-246]

Henceforth, image-assisted surgery will be beneficed by in terms of foreseeingshiftingof the contrast agents, from organic dyes to fluorescent nanoparticles. Enlarging the whole picture, (some) fluorescent nanoparticles can also be flexibly engineered to achieve longer retention times, also accomplish bettermore efficient tumor targeting, provide multimodal imaging readouts and arguably show the way to supply non-morphological data.[247-251] It is a reasonable bet to assume

that fluorescent nanoparticles will substitute existing dye-based probes for clinical applications of fluorescence imaging, those being surgery procedurals and SLN mapping, within the next decade.

AUTHOR INFORMATION

Corresponding Author

Daniel Jaque (daniel.jaque@uam.es) and Riccardo Marin (riccardo.marin@uam.es).

Author Contributions

The manuscript was written through contributions of all authors. All authors have given approval to the final version of the manuscript.

Funding Sources

European Commission: Horizon 2020 Marie Skłodowska-Curie Actions. Grant Number: 797945

European Union's Horizon 2020. Grant Number: 801305

Juan de la Cierva Formación scholarship. Grant Number: FJC2018-036734-I

Ministerio de Economía y Competitividad of Spain. Grant Number: MAT2016-75362-C3-1-R

Ministerio de Ciencia e Innovacion of Spain. Grant Number: PID2019-106211RB-I00.

Comunidad Autónoma de Madrid. Grant Number: B2017/ BMD-3867 RENIM-CM.

Notes

Any additional relevant notes should be placed here.

ACKNOWLEDGMENT

(Word Style “TD_Acknowledgments”).

This work has been co-financed by European Structural and Investment Fund and by the European Union's Horizon 2020 FET Open programme under grant agreement Nº 801305 (NanoTBTech). E.X. is grateful for a Juan de la Cierva Formación scholarship (FJC2018-036734-I). A.B. acknowledges funding from Comunidad de Madrid through TALENTO grant ref. 2019-T1/IND-14014. D.J acknowledges the Ministerio de Economía y Competitividad-MINECO (MAT2016-75362-C3-1-R), the Ministerio de Ciencia e Innovacion of Spain (PID2019-106211RB-I00) and the Comunidad de Madrid (B2017/ BMD-3867 RENIM-CM) R.M. acknowledges the support of the European Commission through the European Union’s Horizon 2020 research and innovation program under the Marie Skłodowska-Curie Grant agreement Nº 797945 (LANTERNS).

ABBREVIATIONS

CCR2, CC chemokine receptor 2; CCL2, CC chemokine ligand 2; CCR5, CC chemokine receptor 5; TLC, thin layer chromatography.

REFERENCES

1. Huang, D.; Swanson, E. A.; Lin, C. P.; Schuman, J. S.; Stinson, W. G.; Chang, W.; Hee, M. R.; Flotte, T.; Gregory, K.; Puliafito, C. A.; et al., Optical coherence tomography. *Science* **1991,** *254* (5035), 1178-81.

2. Sevick-Muraca, E. M.; Lopez, G.; Reynolds, J. S.; Troy, T. L.; Hutchinson, C. L., Fluorescence and absorption contrast mechanisms for biomedical optical imaging using frequency-domain techniques. *Photochem Photobiol* **1997,** *66* (1), 55-64.
3. Yuan, B.; Burgess, S. A.; Iranmahboob, A.; Bouchard, M. B.; Lehrer, N.; Bordier, C.; Hillman, E. M., A system for high-resolution depth-resolved optical imaging of fluorescence and absorption contrast. *Rev Sci Instrum* **2009,** *80* (4), 043706.
4. Marin, R.; Lifante, J.; Besteiro, L. V.; Wang, Z.; Govorov, A. O.; Rivero, F.; Alfonso, F.; Sanz-Rodriguez, F.; Jaque, D., Plasmonic Copper Sulfide Nanoparticles Enable Dark Contrast in Optical Coherence Tomography. *Adv Healthc Mater* **2020,** *9* (5), e1901627.
5. Liu, Y.; Bhattarai, P.; Dai, Z.; Chen, X., Photothermal therapy and photoacoustic imaging via nanotheranostics in fighting cancer. *Chem Soc Rev* **2019,** *48* (7), 2053-2108.
6. Abbaci, M.; Conversano, A.; De Leeuw, F.; Laplace-Builhe, C.; Mazouni, C., Near-infrared fluorescence imaging for the prevention and management of breast cancer-related lymphedema: A systematic review. *Eur J Surg Oncol* **2019,** *45* (10), 1778-1786.
7. AV, D. S.; Lin, H.; Henderson, E. R.; Samkoe, K. S.; Pogue, B. W., Review of fluorescence guided surgery systems: identification of key performance capabilities beyond indocyanine green imaging. *J Biomed Opt* **2016,** *21* (8), 80901.
8. Weber, J.; Beard, P. C.; Bohndiek, S. E., Contrast agents for molecular photoacoustic imaging. *Nat Methods* **2016,** *13* (8), 639-50.
9. Jiang, Y.; Pu, K., Molecular Fluorescence and Photoacoustic Imaging in the Second Near-Infrared Optical Window Using Organic Contrast Agents. *Advanced Biosystems* **2018,** *2* (5).
10. Kenry; Duan, Y.; Liu, B., Recent Advances of Optical Imaging in the Second Near-Infrared Window. *Adv Mater* **2018,** *30* (47), e1802394.
11. Cole, A. J.; Yang, V. C.; David, A. E., Cancer theranostics: the rise of targeted magnetic nanoparticles. *Trends Biotechnol* **2011,** *29* (7), 323-32.
12. Xie, J.; Lee, S.; Chen, X., Nanoparticle-based theranostic agents. *Adv Drug Deliv Rev* **2010,** *62* (11), 1064-79.
13. Skripka, A.; Karabanovas, V.; Jarockyte, G.; Marin, R.; Tam, V.; Cerruti, M.; Rotomskis, R.; Vetrone, F., Decoupling Theranostics with Rare Earth Doped Nanoparticles. *Advanced Functional Materials* **2019,** *29* (12).
14. Schmitz-Valckenberg, S.; Lara, D.; Nizari, S.; Normando, E. M.; Guo, L.; Wegener, A. R.; Tufail, A.; Fitzke, F. W.; Holz, F. G.; Cordeiro, M. F., Localisation and significance of in vivo near-infrared autofluorescent signal in retinal imaging. **2011,** *95* (8), 1134-1139.
15. Croce, A. C.; Bottiroli, G., Autofluorescence spectroscopy and imaging: a tool for biomedical research and diagnosis. *European Journal of Histochemistry* **2014,** *58* (4).
16. Jacques, S. L., Optical properties of biological tissues: a review. *Phys Med Biol* **2013,** *58* (11), R37-61.
17. Bashkatov, A. N.; Genina, E. A.; Kochubey, V. I.; Tuchin, V. V., Optical properties of human skin, subcutaneous and mucous tissues in the wavelength range from 400 to 2000 nm. *Journal of Physics D: Applied Physics* **2005,** *38* (15), 2543-2555.
18. Jaque, D.; Richard, C.; Viana, B.; Soga, K.; Liu, X.; García Solé, J., Inorganic nanoparticles for optical bioimaging. *Adv. Opt. Photon.* **2016,** *8* (1), 1-103.
19. Effects of Ionizing Radiation on Biological Molecules—Mechanisms of Damage and Emerging Methods of Detection. **2014,** *21* (2), 260-292.

20. Lee, D.-E.; Koo, H.; Sun, I.-C.; Ryu, J. H.; Kim, K.; Kwon, I. C., Multifunctional nanoparticles for multimodal imaging and theragnosis. *Chemical Society Reviews* **2012,** *41* (7), 2656-2672.
21. Sharma, P.; Brown, S.; Walter, G.; Santra, S.; Moudgil, B., Nanoparticles for bioimaging. *Advances in Colloid and Interface Science* **2006,** *123-126*, 471-485.
22. Mout, R.; Moyano, D. F.; Rana, S.; Rotello, V. M., Surface functionalization of nanoparticles for nanomedicine. *Chemical Society Reviews* **2012,** *41* (7), 2539-2544.
23. Villa, I.; Vedda, A.; Cantarelli, I. X.; Pedroni, M.; Piccinelli, F.; Bettinelli, M.; Speghini, A.; Quintanilla, M.; Vetrone, F.; Rocha, U.; Jacinto, C.; Carrasco, E.; Rodríguez, F. S.; Juarranz, Á.; del Rosal, B.; Ortgies, D. H.; Gonzalez, P. H.; Solé, J. G.; García, D. J., 1.3 μm emitting SrF2:Nd3+ nanoparticles for high contrast in vivo imaging in the second biological window. *Nano Research* **2015,** *8* (2), 649-665.
24. Diao, S.; Hong, G.; Antaris, A. L.; Blackburn, J. L.; Cheng, K.; Cheng, Z.; Dai, H., Biological imaging without autofluorescence in the second near-infrared region. *Nano Research* **2015,** *8* (9), 3027-3034.
25. Smith, A. M.; Mancini, M. C.; Nie, S., Bioimaging: second window for in vivo imaging. *Nature nanotechnology* **2009,** *4* (11), 710-711.
26. Hemmer, E.; Benayas, A.; Legare, F.; Vetrone, F., Exploiting the biological windows: current perspectives on fluorescent bioprobes emitting above 1000 nm. *Nanoscale Horiz* **2016,** *1* (3), 168-184.
27. Welsher, K.; Sherlock, S. P.; Dai, H., Deep-tissue anatomical imaging of mice using carbon nanotube fluorophores in the second near-infrared window. **2011,** *108* (22), 8943-8948.
28. Naczynski, D. J.; Tan, M. C.; Zevon, M.; Wall, B.; Kohl, J.; Kulesa, A.; Chen, S.; Roth, C. M.; Riman, R. E.; Moghe, P. V., Rare-earth-doped biological composites as in vivo shortwave infrared reporters. *Nature Communications* **2013,** *4* (1), 2199.
29. Hong, G.; Robinson, J. T.; Zhang, Y.; Diao, S.; Antaris, A. L.; Wang, Q.; Dai, H., In vivo fluorescence imaging with Ag2S quantum dots in the second near-infrared region. *Angew Chem Int Ed Engl* **2012,** *51* (39), 9818-21.
30. Zhang, Y.; Hong, G.; Zhang, Y.; Chen, G.; Li, F.; Dai, H.; Wang, Q., Ag2S quantum dot: a bright and biocompatible fluorescent nanoprobe in the second near-infrared window. *ACS Nano* **2012,** *6* (5), 3695-702.
31. Zhong, Y.; Ma, Z.; Zhu, S.; Yue, J.; Zhang, M.; Antaris, A. L.; Yuan, J.; Cui, R.; Wan, H.; Zhou, Y.; Wang, W.; Huang, N. F.; Luo, J.; Hu, Z.; Dai, H., Boosting the down-shifting luminescence of rare-earth nanocrystals for biological imaging beyond 1500 nm. *Nat Commun* **2017,** *8* (1), 737.
32. Santos, H. D. A.; Zabala Gutierrez, I.; Shen, Y.; Lifante, J.; Ximendes, E.; Laurenti, M.; Mendez-Gonzalez, D.; Melle, S.; Calderon, O. G.; Lopez Cabarcos, E.; Fernandez, N.; Chaves-Coira, I.; Lucena-Agell, D.; Monge, L.; Mackenzie, M. D.; Marques-Hueso, J.; Jones, C. M. S.; Jacinto, C.; Del Rosal, B.; Kar, A. K.; Rubio-Retama, J.; Jaque, D., Ultrafast photochemistry produces superbright short-wave infrared dots for low-dose in vivo imaging. *Nat Commun* **2020,** *11* (1), 2933.
33. Li, C.; Zhang, Y.; Wang, M.; Zhang, Y.; Chen, G.; Li, L.; Wu, D.; Wang, Q., In vivo real-time visualization of tissue blood flow and angiogenesis using Ag2S quantum dots in the NIR-II window. *Biomaterials* **2014,** *35* (1), 393-400.
34. Bruns, O. T.; Bischof, T. S.; Harris, D. K.; Franke, D.; Shi, Y.; Riedemann, L.; Bartelt, A.; Jaworski, F. B.; Carr, J. A.; Rowlands, C. J.; Wilson, M. W. B.; Chen, O.; Wei,

H.; Hwang, G. W.; Montana, D. M.; Coropceanu, I.; Achorn, O. B.; Kloepper, J.; Heeren, J.; So, P. T. C.; Fukumura, D.; Jensen, K. F.; Jain, R. K.; Bawendi, M. G., Next-generation in vivo optical imaging with short-wave infrared quantum dots. *Nat Biomed Eng* **2017,** *1*.
35. Angelo, J.; Chen, S.-J.; Ochoa, M.; Sunar, U.; Gioux, S.; Intes, X., Review of structured light in diffuse optical imaging. **2018,** *24 %J Journal of Biomedical Optics* (7), 071602.
36. Umezawa, M.; Sera, T.; Yokota, H.; Takematsu, M.; Morita, M.; Yeroslavsky, G.; Kamimura, M.; Soga, K., Computed tomography for in vivo deep over-1000 nm near-infrared fluorescence imaging. **2020,** *13* (8), e202000071.
37. Peng, P.; Wu, N.; Ye, L.; Jiang, F.; Feng, W.; Li, F.; Liu, Y.; Hong, M., Biodegradable Inorganic Upconversion Nanocrystals for In Vivo Applications. *ACS Nano* **2020**.
38. Lisjak, D.; Plohl, O.; Vidmar, J.; Majaron, B.; Ponikvar-Svet, M., Dissolution Mechanism of Upconverting AYF4:Yb,Tm (A = Na or K) Nanoparticles in Aqueous Media. *Langmuir* **2016,** *32* (32), 8222-9.
39. Palo, E.; Zhang, H.; Lastusaari, M.; Salomäki, M., Nanometer-Thick Ion-Selective Polyelectrolyte Multilayer Coatings to Inhibit the Disintegration of Inorganic Upconverting Nanoparticles. *ACS Applied Nano Materials* **2020,** *3* (7), 6892-6898.
40. Lahtinen, S.; Lyytikäinen, A.; Päkkilä, H.; Hömppi, E.; Perälä, N.; Lastusaari, M.; Soukka, T., Disintegration of Hexagonal NaYF4:Yb3+,Er3+ Upconverting Nanoparticles in Aqueous Media: The Role of Fluoride in Solubility Equilibrium. *The Journal of Physical Chemistry C* **2016,** *121* (1), 656-665.
41. Plohl, O.; Kraft, M.; Kovac, J.; Belec, B.; Ponikvar-Svet, M.; Wurth, C.; Lisjak, D.; Resch-Genger, U., Optically Detected Degradation of NaYF4:Yb,Tm-Based Upconversion Nanoparticles in Phosphate Buffered Saline Solution. *Langmuir* **2017,** *33* (2), 553-560.
42. De Jong, W. H.; Hagens, W. I.; Krystek, P.; Burger, M. C.; Sips, A. J.; Geertsma, R. E., Particle size-dependent organ distribution of gold nanoparticles after intravenous administration. *Biomaterials* **2008,** *29* (12), 1912-9.
43. Mijnendonckx, K.; Leys, N.; Mahillon, J.; Silver, S.; Van Houdt, R., Antimicrobial silver: uses, toxicity and potential for resistance. *Biometals* **2013,** *26* (4), 609-21.
44. Gaetke, L., Copper toxicity, oxidative stress, and antioxidant nutrients. *Toxicology* **2003,** *189* (1-2), 147-163.
45. Zhang, Y. N.; Poon, W.; Tavares, A. J.; McGilvray, I. D.; Chan, W. C. W., Nanoparticle-liver interactions: Cellular uptake and hepatobiliary elimination. *J Control Release* **2016,** *240*, 332-348.
46. Boey, A.; Ho, H. K., All Roads Lead to the Liver: Metal Nanoparticles and Their Implications for Liver Health. *Small* **2020,** *16* (21), e2000153.
47. Poon, W.; Zhang, Y. N.; Ouyang, B.; Kingston, B. R.; Wu, J. L. Y.; Wilhelm, S.; Chan, W. C. W., Elimination Pathways of Nanoparticles. *ACS Nano* **2019,** *13* (5), 5785-5798.
48. Ermolin, M. S.; Fedotov, P. S.; Malik, N. A.; Karandashev, V. K., Nanoparticles of volcanic ash as a carrier for toxic elements on the global scale. *Chemosphere* **2018,** *200*, 16-22.
49. Yang, Y.; Vance, M.; Tou, F.; Tiwari, A.; Liu, M.; Hochella, M. F., Nanoparticles in road dust from impervious urban surfaces: distribution, identification, and environmental implications. *Environmental Science: Nano* **2016,** *3* (3), 534-544.
50. Uebe, R.; Schuler, D., Magnetosome biogenesis in magnetotactic bacteria. *Nat Rev Microbiol* **2016,** *14* (10), 621-37.

51. Jayaweera, M.; Perera, H.; Gunawardana, B.; Manatunge, J., Transmission of COVID-19 virus by droplets and aerosols: A critical review on the unresolved dichotomy. *Environ Res* **2020,** *188*, 109819.
52. Donaldson, K.; Stone, V.; Tran, C. L.; Kreyling, W.; Borm, P. J., Nanotoxicology. *Occup Environ Med* **2004,** *61* (9), 727-8.
53. Wilsdon, J., The politics of small things: nanotechnology, risk, and uncertainty. *IEEE Technology and Society Magazine* **2004,** *23* (4), 16-21.
54. Colvin, V. L., The potential environmental impact of engineered nanomaterials. *Nat Biotechnol* **2003,** *21* (10), 1166-70.
55. Jani, P.; Halbert, G. W.; Langridge, J.; Florence, A. T., Nanoparticle uptake by the rat gastrointestinal mucosa: quantitation and particle size dependency. *J Pharm Pharmacol* **1990,** *42* (12), 821-6.
56. Utell, M. J.; Frampton, M. W., Acute health effects of ambient air pollution: the ultrafine particle hypothesis. *J Aerosol Med* **2000,** *13* (4), 355-59.
57. Ferin, J.; OberdÖRster, G., Translocation of Particles from Pulmonary Alveoli into the Interstitium*. *Journal of Aerosol Medicine* **1992,** *5* (3), 179-187.
58. Tan, M. H.; Commens, C. A.; Burnett, L.; Snitch, P. J., A pilot study on the percutaneous absorption of microfine titanium dioxide from sunscreens. *Australas J Dermatol* **1996,** *37* (4), 185-7.
59. Oberdorster, G.; Utell, M. J., Ultrafine particles in the urban air: to the respiratory tract--and beyond? *Environ Health Perspect* **2002,** *110* (8), A440-1.
60. Choi, H. S.; Ashitate, Y.; Lee, J. H.; Kim, S. H.; Matsui, A.; Insin, N.; Bawendi, M. G.; Semmler-Behnke, M.; Frangioni, J. V.; Tsuda, A., Rapid translocation of nanoparticles from the lung airspaces to the body. *Nat Biotechnol* **2010,** *28* (12), 1300-3.
61. Kreyling, W. G.; Hirn, S.; Schleh, C., Nanoparticles in the lung. *Nat Biotechnol* **2010,** *28* (12), 1275-6.
62. Hagens, W. I.; Oomen, A. G.; de Jong, W. H.; Cassee, F. R.; Sips, A. J., What do we (need to) know about the kinetic properties of nanoparticles in the body? *Regul Toxicol Pharmacol* **2007,** *49* (3), 217-29.
63. Ban, Z.; Zhou, Q.; Sun, A.; Mu, L.; Hu, X., Screening Priority Factors Determining and Predicting the Reproductive Toxicity of Various Nanoparticles. *Environ Sci Technol* **2018,** *52* (17), 9666-9676.
64. Millstone, J. E.; Chan, W. C. W.; Kagan, C. R.; Liz-Marzan, L. M.; Kotov, N. A.; Mulvaney, P. A.; Parak, W. J.; Rogach, A. L.; Weiss, P. S.; Schaak, R. E., Redefining the Experimental and Methods Sections. *ACS Nano* **2019,** *13* (5), 4862-4864.
65. Join the dialogue. *Nat Nanotechnol* **2012,** *7* (9), 545.
66. Lammers, T.; Storm, G., Setting standards to promote progress in bio-nano science. *Nat Nanotechnol* **2019,** *14* (7), 626.
67. Faria, M.; Bjornmalm, M.; Thurecht, K. J.; Kent, S. J.; Parton, R. G.; Kavallaris, M.; Johnston, A. P. R.; Gooding, J. J.; Corrie, S. R.; Boyd, B. J.; Thordarson, P.; Whittaker, A. K.; Stevens, M. M.; Prestidge, C. A.; Porter, C. J. H.; Parak, W. J.; Davis, T. P.; Crampin, E. J.; Caruso, F., Minimum information reporting in bio-nano experimental literature. *Nat Nanotechnol* **2018,** *13* (9), 777-785.
68. Leong, H. S.; Butler, K. S.; Brinker, C. J.; Azzawi, M.; Conlan, S.; Dufes, C.; Owen, A.; Rannard, S.; Scott, C.; Chen, C.; Dobrovolskaia, M. A.; Kozlov, S. V.; Prina-Mello, A.; Schmid, R.; Wick, P.; Caputo, F.; Boisseau, P.; Crist, R. M.; McNeil, S. E.; Fadeel, B.; Tran,

L.; Hansen, S. F.; Hartmann, N. B.; Clausen, L. P. W.; Skjolding, L. M.; Baun, A.; Agerstrand, M.; Gu, Z.; Lamprou, D. A.; Hoskins, C.; Huang, L.; Song, W.; Cao, H.; Liu, X.; Jandt, K. D.; Jiang, W.; Kim, B. Y. S.; Wheeler, K. E.; Chetwynd, A. J.; Lynch, I.; Moghimi, S. M.; Nel, A.; Xia, T.; Weiss, P. S.; Sarmento, B.; das Neves, J.; Santos, H. A.; Santos, L.; Mitragotri, S.; Little, S.; Peer, D.; Amiji, M. M.; Alonso, M. J.; Petri-Fink, A.; Balog, S.; Lee, A.; Drasler, B.; Rothen-Rutishauser, B.; Wilhelm, S.; Acar, H.; Harrison, R. G.; Mao, C.; Mukherjee, P.; Ramesh, R.; McNally, L. R.; Busatto, S.; Wolfram, J.; Bergese, P.; Ferrari, M.; Fang, R. H.; Zhang, L.; Zheng, J.; Peng, C.; Du, B.; Yu, M.; Charron, D. M.; Zheng, G.; Pastore, C., On the issue of transparency and reproducibility in nanomedicine. *Nat Nanotechnol* **2019,** *14* (7), 629-635.
69. Winkler, D. A.; Mombelli, E.; Pietroiusti, A.; Tran, L.; Worth, A.; Fadeel, B.; McCall, M. J., Applying quantitative structure-activity relationship approaches to nanotoxicology: current status and future potential. *Toxicology* **2013,** *313* (1), 15-23.
70. Lazarovits, J.; Sindhwani, S.; Tavares, A. J.; Zhang, Y.; Song, F.; Audet, J.; Krieger, J. R.; Syed, A. M.; Stordy, B.; Chan, W. C. W., Supervised Learning and Mass Spectrometry Predicts the in Vivo Fate of Nanomaterials. *ACS Nano* **2019,** *13* (7), 8023-8034.
71. End-of-life. https://eur-lex.europa.eu/legal-content/EN/ALL/?uri=CELEX:32000L0053.
72. https://ec.europa.eu/commission/presscorner/detail/en/IP_06_903.
73. Hanifi, D. A.; Bronstein, N. D.; Koscher, B. A.; Nett, Z.; Swabeck, J. K.; Takano, K.; Schwartzberg, A. M.; Maserati, L.; Vandewal, K.; van de Burgt, Y.; Salleo, A.; Alivisatos, A. P., Redefining near-unity luminescence in quantum dots with photothermal threshold quantum yield. *Science* **2019,** *363* (6432), 1199-1202.
74. Benayas, A.; Ren, F.; Carrasco, E.; Marzal, V.; del Rosal, B.; Gonfa, B. A.; Juarranz, Á.; Sanz-Rodríguez, F.; Jaque, D.; García-Solé, J.; Ma, D.; Vetrone, F., PbS/CdS/ZnS Quantum Dots: A Multifunctional Platform for In Vivo Near-Infrared Low-Dose Fluorescence Imaging. *Advanced Functional Materials* **2015,** *25* (42), 6650-6659.
75. Amendment.
76. Liu, Y.; Tourbin, M.; Lachaize, S.; Guiraud, P., Nanoparticles in wastewaters: Hazards, fate and remediation. *Powder Technology* **2014,** *255*, 149-156.
77. Rim, K. T.; Koo, K. H.; Park, J. S., Toxicological evaluations of rare earths and their health impacts to workers: a literature review. *Saf Health Work* **2013,** *4* (1), 12-26.
78. Gnach, A.; Lipinski, T.; Bednarkiewicz, A.; Rybka, J.; Capobianco, J. A., Upconverting nanoparticles: assessing the toxicity. *Chem Soc Rev* **2015,** *44* (6), 1561-84.
79. Zhang, M.; Yue, J.; Cui, R.; Ma, Z.; Wan, H.; Wang, F.; Zhu, S.; Zhou, Y.; Kuang, Y.; Zhong, Y.; Pang, D. W.; Dai, H., Bright quantum dots emitting at approximately 1,600 nm in the NIR-IIb window for deep tissue fluorescence imaging. *Proc Natl Acad Sci U S A* **2018,** *115* (26), 6590-6595.
80. Chen, J.; Kong, Y.; Wang, W.; Fang, H.; Wo, Y.; Zhou, D.; Wu, Z.; Li, Y.; Chen, S., Direct water-phase synthesis of lead sulfide quantum dots encapsulated by beta-lactoglobulin for in vivo second near infrared window imaging with reduced toxicity. *Chem Commun (Camb)* **2016,** *52* (21), 4025-8.
81. Shi, X.; Chen, S.; Luo, M.-Y.; Huang, B.; Zhang, G.; Cui, R.; Zhang, M., Zn-doping enhances the photoluminescence and stability of PbS quantum dots for in vivo high-resolution imaging in the NIR-II window. *Nano Research* **2020,** *13* (8), 2239-2245.

82. Wang, D.; Qian, J.; Cai, F.; He, S.; Han, S.; Mu, Y., 'Green'-synthesized near-infrared PbS quantum dots with silica-PEG dual-layer coating: ultrastable and biocompatible optical probes for in vivo animal imaging. *Nanotechnology* **2012,** *23* (24), 245701.
83. Hu, R.; Law, W. C.; Lin, G.; Ye, L.; Liu, J.; Liu, J.; Reynolds, J. L.; Yong, K. T., PEGylated Phospholipid Micelle-Encapsulated Near-Infrared PbS Quantum Dots for in vitro and in vivo Bioimaging. *Theranostics* **2012,** *2* (7), 723-33.
84. Kong, Y.; Chen, J.; Fang, H.; Heath, G.; Wo, Y.; Wang, W.; Li, Y.; Guo, Y.; Evans, S. D.; Chen, S.; Zhou, D., Highly Fluorescent Ribonuclease-A-Encapsulated Lead Sulfide Quantum Dots for Ultrasensitive Fluorescence in Vivo Imaging in the Second Near-Infrared Window. *Chem Mater* **2016,** *28* (9), 3041-3050.
85. Zamberlan, F.; Turyanska, L.; Patane, A.; Liu, Z.; Williams, H. E. L.; Fay, M. W.; Clarke, P. A.; Imamura, Y.; Jin, T.; Bradshaw, T. D.; Thomas, N. R.; Grabowska, A. M., Stable DHLA-PEG capped PbS quantum dots: from synthesis to near-infrared biomedical imaging. *J Mater Chem B* **2018,** *6* (4), 550-555.
86. Qiu, X.; Zhu, X.; Su, X.; Xu, M.; Yuan, W.; Liu, Q.; Xue, M.; Liu, Y.; Feng, W.; Li, F., Near-Infrared Upconversion Luminescence and Bioimaging In Vivo Based on Quantum Dots. *Adv Sci (Weinh)* **2019,** *6* (5), 1801834.
87. Cotruvo, J. A., Jr., The Chemistry of Lanthanides in Biology: Recent Discoveries, Emerging Principles, and Technological Applications. *ACS Cent Sci* **2019,** *5* (9), 1496-1506.
88. Dabbousi, B. O.; Rodriguez-Viejo, J.; Mikulec, F. V.; Heine, J. R.; Mattoussi, H.; Ober, R.; Jensen, K. F.; Bawendi, M. G., (CdSe)ZnS Core−Shell Quantum Dots: Synthesis and Characterization of a Size Series of Highly Luminescent Nanocrystallites. *The Journal of Physical Chemistry B* **1997,** *101* (46), 9463-9475.
89. Chen, G.; Shen, J.; Ohulchanskyy, T. Y.; Patel, N. J.; Kutikov, A.; Li, Z.; Song, J.; Pandey, R. K.; Agren, H.; Prasad, P. N.; Han, G., (alpha-NaYbF4:Tm(3+))/CaF2 core/shell nanoparticles with efficient near-infrared to near-infrared upconversion for high-contrast deep tissue bioimaging. *ACS Nano* **2012,** *6* (9), 8280-7.
90. Ding, H.; Zhou, X.; Qin, B.; Zhou, Z.; Zhao, Y., Highly fluorescent near-infrared emitting carbon dots derived from lemon juice and its bioimaging application. *Journal of Luminescence* **2019,** *211*, 298-304.
91. Bao, X.; Yuan, Y.; Chen, J.; Zhang, B.; Li, D.; Zhou, D.; Jing, P.; Xu, G.; Wang, Y.; Hola, K.; Shen, D.; Wu, C.; Song, L.; Liu, C.; Zboril, R.; Qu, S., In vivo theranostics with near-infrared-emitting carbon dots-highly efficient photothermal therapy based on passive targeting after intravenous administration. *Light Sci Appl* **2018,** *7*, 91.
92. Ding, H.; Yu, S. B.; Wei, J. S.; Xiong, H. M., Full-Color Light-Emitting Carbon Dots with a Surface-State-Controlled Luminescence Mechanism. *ACS Nano* **2016,** *10* (1), 484-91.
93. Bian, W.; Lin, Y.; Wang, T.; Yu, X.; Qiu, J.; Zhou, M.; Luo, H.; Yu, S. F.; Xu, X., Direct Identification of Surface Defects and Their Influence on the Optical Characteristics of Upconversion Nanoparticles. *ACS Nano* **2018,** *12* (4), 3623-3628.
94. Rivest, J. B.; Jain, P. K., Cation exchange on the nanoscale: an emerging technique for new material synthesis, device fabrication, and chemical sensing. *Chem Soc Rev* **2013,** *42* (1), 89-96.
95. Bogdan, N.; Vetrone, F.; Ozin, G. A.; Capobianco, J. A., Synthesis of ligand-free colloidally stable water dispersible brightly luminescent lanthanide-doped upconverting nanoparticles. *Nano Lett* **2011,** *11* (2), 835-40.

96. Ivask, A.; Kurvet, I.; Kasemets, K.; Blinova, I.; Aruoja, V.; Suppi, S.; Vija, H.; Kakinen, A.; Titma, T.; Heinlaan, M.; Visnapuu, M.; Koller, D.; Kisand, V.; Kahru, A., Size-dependent toxicity of silver nanoparticles to bacteria, yeast, algae, crustaceans and mammalian cells in vitro. *PLoS One* **2014,** *9* (7), e102108.
97. Senut, M. C.; Zhang, Y.; Liu, F.; Sen, A.; Ruden, D. M.; Mao, G., Size-Dependent Toxicity of Gold Nanoparticles on Human Embryonic Stem Cells and Their Neural Derivatives. *Small* **2016,** *12* (5), 631-46.
98. Karlsson, H. L.; Gustafsson, J.; Cronholm, P.; Moller, L., Size-dependent toxicity of metal oxide particles--a comparison between nano- and micrometer size. *Toxicol Lett* **2009,** *188* (2), 112-8.
99. Betzer, O.; Shilo, M.; Opochinsky, R.; Barnoy, E.; Motiei, M.; Okun, E.; Yadid, G.; Popovtzer, R., The effect of nanoparticle size on the ability to cross the blood-brain barrier: an in vivo study. *Nanomedicine (Lond)* **2017,** *12* (13), 1533-1546.
100. Gao, K.; Jiang, X., Influence of particle size on transport of methotrexate across blood brain barrier by polysorbate 80-coated polybutylcyanoacrylate nanoparticles. *Int J Pharm* **2006,** *310* (1-2), 213-9.
101. Guo, Y.; Terazzi, E.; Seemann, R.; Fleury, J. B.; Baulin, V. A., Direct proof of spontaneous translocation of lipid-covered hydrophobic nanoparticles through a phospholipid bilayer. *Sci Adv* **2016,** *2* (11), e1600261.
102. Villanueva-Flores, F.; Castro-Lugo, A.; Ramirez, O. T.; Palomares, L. A., Understanding cellular interactions with nanomaterials: towards a rational design of medical nanodevices. *Nanotechnology* **2020,** *31* (13), 132002.
103. Singh, R. P.; Das, M.; Thakare, V.; Jain, S., Functionalization density dependent toxicity of oxidized multiwalled carbon nanotubes in a murine macrophage cell line. *Chem Res Toxicol* **2012,** *25* (10), 2127-37.
104. Albanese, A.; Chan, W. C., Effect of gold nanoparticle aggregation on cell uptake and toxicity. *ACS Nano* **2011,** *5* (7), 5478-89.
105. Yang, J. A.; Lohse, S. E.; Murphy, C. J., Tuning cellular response to nanoparticles via surface chemistry and aggregation. *Small* **2014,** *10* (8), 1642-51.
106. Tripathy, N.; Hong, T. K.; Ha, K. T.; Jeong, H. S.; Hahn, Y. B., Effect of ZnO nanoparticles aggregation on the toxicity in RAW 264.7 murine macrophage. *J Hazard Mater* **2014,** *270*, 110-7.
107. Liu, X.; Chen, Y.; Li, H.; Huang, N.; Jin, Q.; Ren, K.; Ji, J., Enhanced retention and cellular uptake of nanoparticles in tumors by controlling their aggregation behavior. *ACS Nano* **2013,** *7* (7), 6244-57.
108. Li, H.; Chen, Y.; Li, Z.; Li, X.; Jin, Q.; Ji, J., Hemoglobin as a Smart pH-Sensitive Nanocarrier To Achieve Aggregation Enhanced Tumor Retention. *Biomacromolecules* **2018,** *19* (6), 2007-2013.
109. Qian, R. C.; Lv, J.; Long, Y. T., Controllable Aggregation-Induced Exocytosis Inhibition (CAIEI) of Plasmonic Nanoparticles in Cancer Cells Regulated by MicroRNA. *Mol Pharm* **2018,** *15* (9), 4031-4037.
110. Nair, S.; Sasidharan, A.; Divya Rani, V. V.; Menon, D.; Nair, S.; Manzoor, K.; Raina, S., Role of size scale of ZnO nanoparticles and microparticles on toxicity toward bacteria and osteoblast cancer cells. *J Mater Sci Mater Med* **2009,** *20 Suppl 1*, S235-41.
111. Poland, C. A.; Duffin, R.; Kinloch, I.; Maynard, A.; Wallace, W. A.; Seaton, A.; Stone, V.; Brown, S.; Macnee, W.; Donaldson, K., Carbon nanotubes introduced into the

abdominal cavity of mice show asbestos-like pathogenicity in a pilot study. *Nat Nanotechnol* **2008,** *3* (7), 423-8.
112. Harik, V. M., Geometry of carbon nanotubes and mechanisms of phagocytosis and toxic effects. *Toxicol Lett* **2017,** *273*, 69-85.
113. Liu, Y.; Zhao, Y.; Sun, B.; Chen, C., Understanding the toxicity of carbon nanotubes. *Acc Chem Res* **2013,** *46* (3), 702-13.
114. Muller, J.; Huaux, F.; Moreau, N.; Misson, P.; Heilier, J. F.; Delos, M.; Arras, M.; Fonseca, A.; Nagy, J. B.; Lison, D., Respiratory toxicity of multi-wall carbon nanotubes. *Toxicol Appl Pharmacol* **2005,** *207* (3), 221-31.
115. Sun, H.; Jiang, C.; Wu, L.; Bai, X.; Zhai, S., Cytotoxicity-Related Bioeffects Induced by Nanoparticles: The Role of Surface Chemistry. *Front Bioeng Biotechnol* **2019,** *7*, 414.
116. Lin, G.; Chen, T.; Pan, Y.; Yang, Z.; Li, L.; Yong, K. T.; Wang, X.; Wang, J.; Chen, Y.; Jiang, W.; Weng, S.; Huang, X.; Kuang, J.; Xu, G., Biodistribution and acute toxicity of cadmium-free quantum dots with different surface functional groups in mice following intratracheal inhalation. *Nanotheranostics* **2020,** *4* (3), 173-183.
117. Huhn, D.; Kantner, K.; Geidel, C.; Brandholt, S.; De Cock, I.; Soenen, S. J.; Rivera Gil, P.; Montenegro, J. M.; Braeckmans, K.; Mullen, K.; Nienhaus, G. U.; Klapper, M.; Parak, W. J., Polymer-coated nanoparticles interacting with proteins and cells: focusing on the sign of the net charge. *ACS Nano* **2013,** *7* (4), 3253-63.
118. Donahue, N. D.; Acar, H.; Wilhelm, S., Concepts of nanoparticle cellular uptake, intracellular trafficking, and kinetics in nanomedicine. *Adv Drug Deliv Rev* **2019,** *143*, 68-96.
119. Hao, R.; Xing, R.; Xu, Z.; Hou, Y.; Gao, S.; Sun, S., Synthesis, functionalization, and biomedical applications of multifunctional magnetic nanoparticles. *Adv Mater* **2010,** *22* (25), 2729-42.
120. Gupta, A. K.; Naregalkar, R. R.; Vaidya, V. D.; Gupta, M., Recent advances on surface engineering of magnetic iron oxide nanoparticles and their biomedical applications. *Nanomedicine (Lond)* **2007,** *2* (1), 23-39.
121. Mohammed, L.; Gomaa, H. G.; Ragab, D.; Zhu, J., Magnetic nanoparticles for environmental and biomedical applications: A review. *Particuology* **2017,** *30*, 1-14.
122. Wagner, A. M.; Knipe, J. M.; Orive, G.; Peppas, N. A., Quantum dots in biomedical applications. *Acta Biomater* **2019,** *94*, 44-63.
123. Abdul Jalil, R.; Zhang, Y., Biocompatibility of silica coated NaYF(4) upconversion fluorescent nanocrystals. *Biomaterials* **2008,** *29* (30), 4122-8.
124. Sun, L.; Wei, R.; Feng, J.; Zhang, H., Tailored lanthanide-doped upconversion nanoparticles and their promising bioapplication prospects. *Coordination Chemistry Reviews* **2018,** *364*, 10-32.
125. Gerion, D.; Pinaud, F.; Williams, S. C.; Parak, W. J.; Zanchet, D.; Weiss, S.; Alivisatos, A. P., Synthesis and Properties of Biocompatible Water-Soluble Silica-Coated CdSe/ZnS Semiconductor Quantum Dots†. *The Journal of Physical Chemistry B* **2001,** *105* (37), 8861-8871.
126. Drijvers, E.; Liu, J.; Harizaj, A.; Wiesner, U.; Braeckmans, K.; Hens, Z.; Aubert, T., Efficient Endocytosis of Inorganic Nanoparticles with Zwitterionic Surface Functionalization. *ACS Appl Mater Interfaces* **2019,** *11* (42), 38475-38482.
127. Debayle, M.; Balloul, E.; Dembele, F.; Xu, X.; Hanafi, M.; Ribot, F.; Monzel, C.; Coppey, M.; Fragola, A.; Dahan, M.; Pons, T.; Lequeux, N., Zwitterionic polymer ligands: an

ideal surface coating to totally suppress protein-nanoparticle corona formation? *Biomaterials* **2019,** *219*, 119357.
128. Zhang, F.; Lees, E.; Amin, F.; Rivera Gil, P.; Yang, F.; Mulvaney, P.; Parak, W. J., Polymer-coated nanoparticles: a universal tool for biolabelling experiments. *Small* **2011,** *7* (22), 3113-27.
129. Bobo, D.; Robinson, K. J.; Islam, J.; Thurecht, K. J.; Corrie, S. R., Nanoparticle-Based Medicines: A Review of FDA-Approved Materials and Clinical Trials to Date. *Pharm Res* **2016,** *33* (10), 2373-87.
130. Karakoti, A. S.; Das, S.; Thevuthasan, S.; Seal, S., PEGylated inorganic nanoparticles. *Angew Chem Int Ed Engl* **2011,** *50* (9), 1980-94.
131. Roberts, M. J.; Bentley, M. D.; Harris, J. M., Chemistry for peptide and protein PEGylation. *Advanced Drug Delivery Reviews* **2002,** *54* (4), 459-476.
132. Shiraishi, K.; Yokoyama, M., Toxicity and immunogenicity concerns related to PEGylated-micelle carrier systems: a review. *Sci Technol Adv Mater* **2019,** *20* (1), 324-336.
133. Grenier, P.; Viana, I. M. O.; Lima, E. M.; Bertrand, N., Anti-polyethylene glycol antibodies alter the protein corona deposited on nanoparticles and the physiological pathways regulating their fate in vivo. *J Control Release* **2018,** *287*, 121-131.
134. Carrasco, E.; del Rosal, B.; Sanz-Rodríguez, F.; de la Fuente, Á. J.; Gonzalez, P. H.; Rocha, U.; Kumar, K. U.; Jacinto, C.; Solé, J. G.; Jaque, D., Intratumoral Thermal Reading During Photo-Thermal Therapy by Multifunctional Fluorescent Nanoparticles. *Advanced Functional Materials* **2015,** *25* (4), 615-626.
135. Lan, M.; Zhao, S.; Zhang, Z.; Yan, L.; Guo, L.; Niu, G.; Zhang, J.; Zhao, J.; Zhang, H.; Wang, P.; Zhu, G.; Lee, C.-S.; Zhang, W., Two-photon-excited near-infrared emissive carbon dots as multifunctional agents for fluorescence imaging and photothermal therapy. *Nano Research* **2017,** *10* (9), 3113-3123.
136. Al-Jamal, W. T.; Al-Jamal, K. T.; Bomans, P. H.; Frederik, P. M.; Kostarelos, K., Functionalized-quantum-dot-liposome hybrids as multimodal nanoparticles for cancer. *Small* **2008,** *4* (9), 1406-15.
137. Chen, G.; Jaskula-Sztul, R.; Esquibel, C. R.; Lou, I.; Zheng, Q.; Dammalapati, A.; Harrison, A.; Eliceiri, K. W.; Tang, W.; Chen, H.; Gong, S., Neuroendocrine Tumor-Targeted Upconversion Nanoparticle-Based Micelles for Simultaneous NIR-Controlled Combination Chemotherapy and Photodynamic Therapy, and Fluorescence Imaging. *Adv Funct Mater* **2017,** *27* (8).
138. Cho, K.; Wang, X.; Nie, S.; Chen, Z. G.; Shin, D. M., Therapeutic nanoparticles for drug delivery in cancer. *Clin Cancer Res* **2008,** *14* (5), 1310-6.
139. Attia, M. F.; Anton, N.; Wallyn, J.; Omran, Z.; Vandamme, T. F., An overview of active and passive targeting strategies to improve the nanocarriers efficiency to tumour sites. *J Pharm Pharmacol* **2019,** *71* (8), 1185-1198.
140. Zhong, Y.; Meng, F.; Deng, C.; Zhong, Z., Ligand-directed active tumor-targeting polymeric nanoparticles for cancer chemotherapy. *Biomacromolecules* **2014,** *15* (6), 1955-69.
141. Byrne, J. D.; Betancourt, T.; Brannon-Peppas, L., Active targeting schemes for nanoparticle systems in cancer therapeutics. *Adv Drug Deliv Rev* **2008,** *60* (15), 1615-26.
142. Tang, W.; Fan, W.; Lau, J.; Deng, L.; Shen, Z.; Chen, X., Emerging blood-brain-barrier-crossing nanotechnology for brain cancer theranostics. *Chem Soc Rev* **2019,** *48* (11), 2967-3014.

143. Zhou, J.; Kroll, A. V.; Holay, M.; Fang, R. H.; Zhang, L., Biomimetic Nanotechnology toward Personalized Vaccines. *Adv Mater* **2020,** *32* (13), e1901255.
144. Fontana, F.; Shahbazi, M. A.; Liu, D.; Zhang, H.; Makila, E.; Salonen, J.; Hirvonen, J. T.; Santos, H. A., Multistaged Nanovaccines Based on Porous Silicon@Acetalated Dextran@Cancer Cell Membrane for Cancer Immunotherapy. *Adv Mater* **2017,** *29* (7).
145. Rao, L.; Bu, L. L.; Cai, B.; Xu, J. H.; Li, A.; Zhang, W. F.; Sun, Z. J.; Guo, S. S.; Liu, W.; Wang, T. H.; Zhao, X. Z., Cancer Cell Membrane-Coated Upconversion Nanoprobes for Highly Specific Tumor Imaging. *Adv Mater* **2016,** *28* (18), 3460-6.
146. Rao, L.; Yu, G. T.; Meng, Q. F.; Bu, L. L.; Tian, R.; Lin, L. S.; Deng, H.; Yang, W.; Zan, M.; Ding, J.; Li, A.; Xiao, H.; Sun, Z. J.; Liu, W.; Chen, X., Cancer Cell Membrane-Coated Nanoparticles for Personalized Therapy in Patient-Derived Xenograft Models. *Advanced Functional Materials* **2019,** *29* (51).
147. Hu, C. M.; Fang, R. H.; Wang, K. C.; Luk, B. T.; Thamphiwatana, S.; Dehaini, D.; Nguyen, P.; Angsantikul, P.; Wen, C. H.; Kroll, A. V.; Carpenter, C.; Ramesh, M.; Qu, V.; Patel, S. H.; Zhu, J.; Shi, W.; Hofman, F. M.; Chen, T. C.; Gao, W.; Zhang, K.; Chien, S.; Zhang, L., Nanoparticle biointerfacing by platelet membrane cloaking. *Nature* **2015,** *526* (7571), 118-21.
148. Hu, C. M.; Zhang, L.; Aryal, S.; Cheung, C.; Fang, R. H.; Zhang, L., Erythrocyte membrane-camouflaged polymeric nanoparticles as a biomimetic delivery platform. *Proc Natl Acad Sci U S A* **2011,** *108* (27), 10980-5.
149. Bros, M.; Nuhn, L.; Simon, J.; Moll, L.; Mailander, V.; Landfester, K.; Grabbe, S., The Protein Corona as a Confounding Variable of Nanoparticle-Mediated Targeted Vaccine Delivery. *Front Immunol* **2018,** *9*, 1760.
150. Corbo, C.; Molinaro, R.; Parodi, A.; Toledano Furman, N. E.; Salvatore, F.; Tasciotti, E., The impact of nanoparticle protein corona on cytotoxicity, immunotoxicity and target drug delivery. *Nanomedicine (Lond)* **2016,** *11* (1), 81-100.
151. Papi, M.; Caputo, D.; Palmieri, V.; Coppola, R.; Palchetti, S.; Bugli, F.; Martini, C.; Digiacomo, L.; Pozzi, D.; Caracciolo, G., Clinically approved PEGylated nanoparticles are covered by a protein corona that boosts the uptake by cancer cells. *Nanoscale* **2017,** *9* (29), 10327-10334.
152. Del Rosal, B.; Ortgies, D. H.; Fernandez, N.; Sanz-Rodriguez, F.; Jaque, D.; Rodriguez, E. M., Overcoming Autofluorescence: Long-Lifetime Infrared Nanoparticles for Time-Gated In Vivo Imaging. *Adv Mater* **2016,** *28* (46), 10188-10193.
153. Yang, W.; Srivastava, P. K.; Han, S.; Jing, L.; Tu, C. C.; Chen, S. L., Optomechanical Time-Gated Fluorescence Imaging Using Long-Lived Silicon Quantum Dot Nanoparticles. *Anal Chem* **2019,** *91* (9), 5499-5503.
154. Kodama, Y., Time Gating of Chloroplast Autofluorescence Allows Clearer Fluorescence Imaging In Planta. *PLoS One* **2016,** *11* (3), e0152484.
155. Rubin, M. B.; Braslavsky, S. E., Quantum yield: the term and the symbol. A historical search. *Photochem Photobiol Sci* **2010,** *9* (5), 670-4.
156. McNaught, A. D.; Wilkinson, A., *The IUPAC Compendium of Chemical Terminology (2nd edition)*. Blackwell Science: Oxford, England, 1997.
157. Johnson, N. J.; He, S.; Diao, S.; Chan, E. M.; Dai, H.; Almutairi, A., Direct Evidence for Coupled Surface and Concentration Quenching Dynamics in Lanthanide-Doped Nanocrystals. *J Am Chem Soc* **2017,** *139* (8), 3275-3282.

158. Wuister, S. F.; de Mello Donega, C.; Meijerink, A., Luminescence temperature antiquenching of water-soluble CdTe quantum dots: role of the solvent. *J Am Chem Soc* **2004,** *126* (33), 10397-402.
159. Cheng, T.; Marin, R.; Skripka, A.; Vetrone, F., Small and Bright Lithium-Based Upconverting Nanoparticles. *J Am Chem Soc* **2018,** *140* (40), 12890-12899.
160. Boercker, J. E.; Woodall, D. L.; Cunningham, P. D.; Placencia, D.; Ellis, C. T.; Stewart, M. H.; Brintlinger, T. H.; Stroud, R. M.; Tischler, J. G., Synthesis and Characterization of PbS/ZnS Core/Shell Nanocrystals. *Chemistry of Materials* **2018,** *30* (12), 4112-4123.
161. Zang, H.; Li, H.; Makarov, N. S.; Velizhanin, K. A.; Wu, K.; Park, Y. S.; Klimov, V. I., Thick-Shell CuInS2/ZnS Quantum Dots with Suppressed "Blinking" and Narrow Single-Particle Emission Line Widths. *Nano Lett* **2017,** *17* (3), 1787-1795.
162. Shen, Y.; Lifante, J.; Ximendes, E.; Santos, H. D. A.; Ruiz, D.; Juarez, B. H.; Zabala Gutierrez, I.; Torres Vera, V.; Rubio Retama, J.; Martin Rodriguez, E.; Ortgies, D. H.; Jaque, D.; Benayas, A.; Del Rosal, B., Perspectives for Ag2S NIR-II nanoparticles in biomedicine: from imaging to multifunctionality. *Nanoscale* **2019,** *11* (41), 19251-19264.
163. Jiang, L.; Ding, H.; Xu, M.; Hu, X.; Li, S.; Zhang, M.; Zhang, Q.; Wang, Q.; Lu, S.; Tian, Y.; Bi, H., Carbon Dots: UV–Vis–NIR Full-Range Responsive Carbon Dots with Large Multiphoton Absorption Cross Sections and Deep-Red Fluorescence at Nucleoli and In Vivo (Small 19/2020). *Small* **2020,** *16* (19).
164. Marin, R.; Brunet, G.; Murugesu, M., Shining New Light on Multifunctional Lanthanide Single-Molecule Magnets. *Angew Chem Int Ed Engl* **2019**.
165. Zhang, W.; Chen, T.; Su, L.; Ge, X.; Chen, X.; Song, J.; Yang, H., Quantum Dot-Based Sensitization System for Boosted Photon Absorption and Enhanced Second Near-Infrared Luminescence of Lanthanide-Doped Nanoparticle. *Anal Chem* **2020,** *92* (8), 6094-6102.
166. Song, D.; Chi, S.; Li, X.; Wang, C.; Li, Z.; Liu, Z., Upconversion System with Quantum Dots as Sensitizer: Improved Photoluminescence and PDT Efficiency. *ACS Appl Mater Interfaces* **2019,** *11* (44), 41100-41108.
167. Creutz, S. E.; Fainblat, R.; Kim, Y.; De Siena, M. C.; Gamelin, D. R., A Selective Cation Exchange Strategy for the Synthesis of Colloidal Yb(3+)-Doped Chalcogenide Nanocrystals with Strong Broadband Visible Absorption and Long-Lived Near-Infrared Emission. *J Am Chem Soc* **2017,** *139* (34), 11814-11824.
168. Das, A.; Mao, C.; Cho, S.; Kim, K.; Park, W., Over 1000-fold enhancement of upconversion luminescence using water-dispersible metal-insulator-metal nanostructures. *Nat Commun* **2018,** *9* (1), 4828.
169. Ji, B.; Giovanelli, E.; Habert, B.; Spinicelli, P.; Nasilowski, M.; Xu, X.; Lequeux, N.; Hugonin, J. P.; Marquier, F.; Greffet, J. J.; Dubertret, B., Non-blinking quantum dot with a plasmonic nanoshell resonator. *Nat Nanotechnol* **2015,** *10* (2), 170-5.
170. Giannini, V.; Fernandez-Dominguez, A. I.; Heck, S. C.; Maier, S. A., Plasmonic nanoantennas: fundamentals and their use in controlling the radiative properties of nanoemitters. *Chem Rev* **2011,** *111* (6), 3888-912.
171. Smith, M.; Fork, R. L.; Cole, S., Safe delivery of optical power from space. *Opt Express* **2001,** *8* (10), 537-46.
172. Beier, H. T.; Jansen, E. D.; Thomas, R. J.; Kumru, S. S.; Schmidt, M. S.; Boretsky, A. R.; Tijerina, A. J.; Shingledecker, A. D.; Noojin, G. D.; Peterson, A. M.; DeLisi, M. P., Porcine skin damage thresholds for pulsed nanosecond-scale laser exposure at 1064-nm. In *Optical Interactions with Tissue and Cells XXIX*, 2018.

173. Frenz, M.; Mischler, C.; Romano, V.; Forrer, M.; Mller, O. M.; Weber, H. P., Effect of mechanical tissue properties on thermal damage in skin after IR-laser ablation. *Applied Physics B Photophysics and Laser Chemistry* **1991,** *52* (4), 251-258.
174. Ghanmi, A.; Abbas, I. A., An analytical study on the fractional transient heating within the skin tissue during the thermal therapy. *J Therm Biol* **2019,** *82*, 229-233.
175. Golovynskyi, S.; Golovynska, I.; Stepanova, L. I.; Datsenko, O. I.; Liu, L.; Qu, J.; Ohulchanskyy, T. Y., Optical windows for head tissues in near-infrared and short-wave infrared regions: Approaching transcranial light applications. *J Biophotonics* **2018,** *11* (12), e201800141.
176. Wang, M.; Wu, C.; Sinefeld, D.; Li, B.; Xia, F.; Xu, C., Comparing the effective attenuation lengths for long wavelength in vivo imaging of the mouse brain. *Biomed Opt Express* **2018,** *9* (8), 3534-3543.
177. Cheong, W. F.; Prahl, S. A.; Welch, A. J., A review of the optical properties of biological tissues. *IEEE Journal of Quantum Electronics* **1990,** *26* (12), 2166-2185.
178. Smith, A. M.; Mancini, M. C.; Nie, S., Bioimaging: second window for in vivo imaging. *Nat Nanotechnol* **2009,** *4* (11), 710-1.
179. Wang, V. W.; Wu, H.-I., *Biomedical Optics: Principles and Imaging*. Wiley: 2007.
180. Yaroslavsky, A. N.; Schulze, P. C.; Yaroslavsky, I. V.; Schober, R.; Ulrich, F.; Schwarzmaier, H. J., Optical properties of selected native and coagulated human brain tissues in vitro in the visible and near infrared spectral range. *Phys Med Biol* **2002,** *47* (12), 2059-73.
181. Nyk, M.; Kumar, R.; Ohulchanskyy, T. Y.; Bergey, E. J.; Prasad, P. N., High contrast in vitro and in vivo photoluminescence bioimaging using near infrared to near infrared up-conversion in Tm3+ and Yb3+ doped fluoride nanophosphors. *Nano Lett* **2008,** *8* (11), 3834-8.
182. Bashkatov, A. N.; Genina, E. A.; Tuchin, V. V., Optical Properties of Skin, Subcutaneous, and Muscle Tissues: A Review. *Journal of Innovative Optical Health Sciences* **2011,** *04* (01), 9-38.
183. Tozer, B. A., The calculation of maximum permissible exposure levels for laser radiation. *Journal of Physics E: Scientific Instruments* **1979,** *12* (10), 922-922.
184. Yang, K.; Zhang, S.; Zhang, G.; Sun, X.; Lee, S. T.; Liu, Z., Graphene in mice: ultrahigh in vivo tumor uptake and efficient photothermal therapy. *Nano Lett* **2010,** *10* (9), 3318-23.
185. Ximendes, E. C.; Rocha, U.; Jacinto, C.; Kumar, K. U.; Bravo, D.; Lopez, F. J.; Martin Rodriguez, E.; Garcia-Sole, J.; Jaque, D., Self-monitored photothermal nanoparticles based on core-shell engineering. *Nanoscale* **2016,** *8* (5), 3057-66.
186. Ximendes, E. C.; Santos, W. Q.; Rocha, U.; Kagola, U. K.; Sanz-Rodriguez, F.; Fernandez, N.; Gouveia-Neto Ada, S.; Bravo, D.; Domingo, A. M.; del Rosal, B.; Brites, C. D.; Carlos, L. D.; Jaque, D.; Jacinto, C., Unveiling in Vivo Subcutaneous Thermal Dynamics by Infrared Luminescent Nanothermometers. *Nano Lett* **2016,** *16* (3), 1695-703.
187. Li, X.; Jiang, M.; Li, Y.; Xue, Z.; Zeng, S.; Liu, H., 808nm laser-triggered NIR-II emissive rare-earth nanoprobes for small tumor detection and blood vessel imaging. *Mater Sci Eng C Mater Biol Appl* **2019,** *100*, 260-268.
188. Communal, J.-E., Comparing camera sensitivity with Noise Equivalent Irradiance. In *2014 6th Workshop on Hyperspectral Image and Signal Processing: Evolution in Remote Sensing (WHISPERS)*, 2014; pp 1-4.
189. Swartling, J.; Dam, J. S.; Andersson-Engels, S., Comparison of spatially and temporally resolved diffuse-reflectance measurement systems for determination of biomedical optical properties. *Appl Opt* **2003,** *42* (22), 4612-20.

190. Svensson, T.; Swartling, J.; Taroni, P.; Torricelli, A.; Lindblom, P.; Ingvar, C.; Andersson-Engels, S., Characterization of normal breast tissue heterogeneity using time-resolved near-infrared spectroscopy. *Phys Med Biol* **2005,** *50* (11), 2559-71.
191. Tromberg, B. J.; Shah, N.; Lanning, R.; Cerussi, A.; Espinoza, J.; Pham, T.; Svaasand, L.; Butler, J., Non-invasive in vivo characterization of breast tumors using photon migration spectroscopy. *Neoplasia* **2000,** *2* (1-2), 26-40.
192. Tromberg, B. J.; Coquoz, O.; Fishkin, J. B.; Pham, T.; Anderson, E. R.; Butler, J.; Cahn, M.; Gross, J. D.; Venugopalan, V.; Pham, D., Non-invasive measurements of breast tissue optical properties using frequency-domain photon migration. *Philos Trans R Soc Lond B Biol Sci* **1997,** *352* (1354), 661-8.
193. Bays, R.; Wagnières, G.; Robert, D.; Braichotte, D.; Savary, J.-F.; Monnier, P.; van den Bergh, H., Clinical determination of tissue optical properties by endoscopic spatially resolved reflectometry. *Applied Optics* **1996,** *35* (10).
194. Doornbos, R. M.; Lang, R.; Aalders, M. C.; Cross, F. W.; Sterenborg, H. J., The determination of in vivo human tissue optical properties and absolute chromophore concentrations using spatially resolved steady-state diffuse reflectance spectroscopy. *Phys Med Biol* **1999,** *44* (4), 967-81.
195. Pilz, M.; Honold, S.; Kienle, A., Determination of the optical properties of turbid media by measurements of the spatially resolved reflectance considering the point-spread function of the camera system. *J Biomed Opt* **2008,** *13* (5), 054047.
196. Azzi, L.; El-Alfy, M.; Martel, C.; Labrie, F., Gender differences in mouse skin morphology and specific effects of sex steroids and dehydroepiandrosterone. *J Invest Dermatol* **2005,** *124* (1), 22-7.
197. Kowalewska, P. M.; Margetts, P. J.; Fox-Robichaud, A. E., Peritoneal Dialysis Catheter Increases Leukocyte Recruitment in the Mouse Parietal Peritoneum Microcirculation and Causes Fibrosis. *Perit Dial Int* **2016,** *36* (1), 7-15.
198. Richardson, L.; Venkataraman, S.; Stevenson, P.; Yang, Y.; Moss, J.; Graham, L.; Burton, N.; Hill, B.; Rao, J.; Baldock, R. A.; Armit, C., EMAGE mouse embryo spatial gene expression database: 2014 update. *Nucleic Acids Res* **2014,** *42* (Database issue), D835-44.
199. Diot, G.; Metz, S.; Noske, A.; Liapis, E.; Schroeder, B.; Ovsepian, S. V.; Meier, R.; Rummeny, E.; Ntziachristos, V., Multispectral Optoacoustic Tomography (MSOT) of Human Breast Cancer. *Clin Cancer Res* **2017,** *23* (22), 6912-6922.
200. Li, L.; Cazzell, M.; Babawale, O.; Liu, H., Automated voxel classification used with atlas-guided diffuse optical tomography for assessment of functional brain networks in young and older adults. *Neurophotonics* **2016,** *3* (4), 045002.
201. Bosschaart, N.; Leproux, A.; Abdalsalam, O.; Chen, W. P.; McLaren, C. E.; Tromberg, B. J.; O'Sullivan, T. D., Diffuse optical spectroscopic imaging for the investigation of human lactation physiology: a case study on mammary involution. *J Biomed Opt* **2019,** *24* (5), 1-8.
202. Hu, G.; Zhang, Q.; Ivkovic, V.; Strangman, G. E., Ambulatory diffuse optical tomography and multimodality physiological monitoring system for muscle and exercise applications. *J Biomed Opt* **2016,** *21* (9), 091314.
203. Lighter, D.; Hughes, J.; Styles, I.; Filer, A.; Dehghani, H., Multispectral, non-contact diffuse optical tomography of healthy human finger joints. *Biomed Opt Express* **2018,** *9* (4), 1445-1460.

204. Konugolu Venkata Sekar, S.; Pagliazzi, M.; Negredo, E.; Martelli, F.; Farina, A.; Dalla Mora, A.; Lindner, C.; Farzam, P.; Perez-Alvarez, N.; Puig, J.; Taroni, P.; Pifferi, A.; Durduran, T., In Vivo, Non-Invasive Characterization of Human Bone by Hybrid Broadband (600-1200 nm) Diffuse Optical and Correlation Spectroscopies. *PLoS One* **2016,** *11* (12), e0168426.
205. Peelle, J. E., Optical neuroimaging of spoken language. *Lang Cogn Neurosci* **2017,** *32* (7), 847-854.
206. Lee, C. W.; Cooper, R. J.; Austin, T., Diffuse optical tomography to investigate the newborn brain. *Pediatr Res* **2017,** *82* (3), 376-386.
207. Zhu, Q.; Ricci, A., Jr.; Hegde, P.; Kane, M.; Cronin, E.; Merkulov, A.; Xu, Y.; Tavakoli, B.; Tannenbaum, S., Assessment of Functional Differences in Malignant and Benign Breast Lesions and Improvement of Diagnostic Accuracy by Using US-guided Diffuse Optical Tomography in Conjunction with Conventional US. *Radiology* **2016,** *280* (2), 387-97.
208. Fishell, A. K.; Burns-Yocum, T. M.; Bergonzi, K. M.; Eggebrecht, A. T.; Culver, J. P., Mapping brain function during naturalistic viewing using high-density diffuse optical tomography. *Sci Rep* **2019,** *9* (1), 11115.
209. Chalia, M.; Dempsey, L. A.; Cooper, R. J.; Lee, C. W.; Gibson, A. P.; Hebden, J. C.; Austin, T., Diffuse optical tomography for the detection of perinatal stroke at the cot side: a pilot study. *Pediatr Res* **2019,** *85* (7), 1001-1007.
210. Tuchin, V. V.; Bashkatov, A. N.; Genina, E. A.; Kochubey, V. I.; Tuchin, V. V., <title>Optical properties of human cranial bone in the spectral range from 800 to 2000 nm</title>. 2006; pp 616310-616310-11.
211. Oraevsky, A. A.; Sikorski, Z.; Wang, L. V.; Furmanczyk, M.; Przekwas, A. J., Modeling of photon migration in the human lung using a finite volume solver. In *Photons Plus Ultrasound: Imaging and Sensing 2006: The Seventh Conference on Biomedical Thermoacoustics, Optoacoustics, and Acousto-optics*, 2006.
212. Choi, B.; Kollias, N.; Zeng, H.; Kang, H. W.; Wong, B. J. F.; Ilgner, J. F.; Tearney, G. J.; Gregory, K. W.; Marcu, L.; Skala, M. C.; Campagnola, P. J.; Mandelis, A.; Morris, M. D.; Sordillo, D. C.; Sordillo, L. A.; Sordillo, P. P.; Alfano, R. R., Fourth near-infrared optical window for assessment of bone and other tissues. In *Photonic Therapeutics and Diagnostics XII*, 2016.
213. Nogueira, M. S.; Lacerenza, M.; Sekar, S. K. V.; Buttafava, M.; Pifferi, A.; Tosi, A.; Contini, D.; Andersson-Engels, S., Broadband extraction of tissue optical properties using a portable hybrid time-resolved continuous wave instrumentation: characterization of ex vivo organs. In *Biophotonics Congress: Biomedical Optics 2020 (Translational, Microscopy, OCT, OTS, BRAIN)*, 2020.
214. Bashkatov, A. N.; Berezin, K. V.; Dvoretskiy, K. N.; Chernavina, M. L.; Genina, E. A.; Genin, V. D.; Kochubey, V. I.; Lazareva, E. N.; Pravdin, A. B.; Shvachkina, M. E.; Timoshina, P. A.; Tuchina, D. K.; Yakovlev, D. D.; Yakovlev, D. A.; Yanina, I. Y.; Zhernovaya, O. S.; Tuchin, V. V., Measurement of tissue optical properties in the context of tissue optical clearing. *J Biomed Opt* **2018,** *23* (9), 1-31.
215. Cubeddu, R.; D'Andrea, C.; Pifferi, A.; Taroni, P.; Torricelli, A.; Valentini, G., Effects of the Menstrual Cycle on the Red and Near-infrared Optical Properties of the Human Breast ¶. *Photochemistry and Photobiology* **2000,** *72* (3), 383-391.
216. Genina, E. A.; Derbov, V. L.; Meglinski, I.; Tuchin, V. V.; Kozintseva, M. D.; Bashkatov, A. N.; Kochubey, V. I.; Genina, E. A.; Gorodkov, S. Y.; Morozov, D. A.; Tuchin,

V. V., Optical properties of parietal peritoneum in the spectral range 350-2500 nm. In *Saratov Fall Meeting 2013: Optical Technologies in Biophysics and Medicine XV; and Laser Physics and Photonics XV*, 2014.
217. Tuchin, V. V.; Bashkatov, A. N.; Genina, E. A.; Kochubey, V. I.; Gavrilova, A. A.; Kapralov, S. V.; Grishaev, V. A.; Tuchin, V. V., <title>Optical properties of human stomach mucosa in the spectral range from 400 to 2000 nm</title>. 2007; pp 653513-653513-11.
218. Germer, C.-T.; Roggan, A.; Ritz, J. P.; Isbert, C.; Albrecht, D.; Müller, G.; Buhr, H. J., Optical properties of native and coagulated human liver tissue and liver metastases in the near infrared range. *Lasers in Surgery and Medicine* **1998,** *23* (4), 194-203.
219. Ntziachristos, V.; Ripoll, J.; Weissleder, R., Would near-infrared fluorescence signals propagate through large human organs for clinical studies? *Opt Lett* **2002,** *27* (5), 333-5.
220. Ackerman, M. J., The Visible Human Project. *Proceedings of the IEEE* **1998,** *86* (3), 504-511.
221. Ackerman, M. J., The visible human project(R): From body to bits. *Conf Proc IEEE Eng Med Biol Soc* **2016,** *2016*, 3338-3341.
222. Ozsahin, I.; Gharagouzloo, C.; Belov, V.; Alpert, N.; Fakhri, G., Awake animal functional imaging to investigate the effects of general anesthesia on brain. **2018**.
223. Heinke, W.; Koelsch, S., The effects of anesthetics on brain activity and cognitive function. **2005,** *18* (6), 625-631.
224. Alkire, M. T.; Haier, R. J.; Barker, S. J.; Shah, N. K.; Wu, J. C.; Kao, J. Y. J. A. T. J. o. t. A. S. o. A., Cerebral metabolism during propofol anesthesia in humans studied with positron emission tomography. **1995,** *82* (2), 393-403.
225. Park, K.; Chen, W.; Volkow, N. D.; Allen, C. P.; Pan, Y.; Du, C., Hemodynamic and neuronal responses to cocaine differ in awake versus anesthetized animals: Optical brain imaging study. *NeuroImage* **2019,** *188*, 188-197.
226. Kyme, A. Z.; Angelis, G. I.; Eisenhuth, J.; Fulton, R. R.; Zhou, V.; Hart, G.; Popovic, K.; Akhtar, M.; Ryder, W. J.; Clemens, K. J.; Balleine, B. W.; Parmar, A.; Pascali, G.; Perkins, G.; Meikle, S. R., Open-field PET: Simultaneous brain functional imaging and behavioural response measurements in freely moving small animals. *NeuroImage* **2019,** *188*, 92-101.
227. Nath, T.; Mathis, A.; Chen, A. C.; Patel, A.; Bethge, M.; Mathis, M. W., Using DeepLabCut for 3D markerless pose estimation across species and behaviors. *Nature Protocols* **2019,** *14* (7), 2152-2176.
228. Han, J.; Jentzen, A.; E, W., Solving high-dimensional partial differential equations using deep learning. *Proc Natl Acad Sci U S A* **2018,** *115* (34), 8505-8510.
229. Würfl, T.; Ghesu, F. C.; Christlein, V.; Maier, A., Deep Learning Computed Tomography. In *Medical Image Computing and Computer-Assisted Intervention - MICCAI 2016*, 2016; pp 432-440.
230. Lee, H.; Huang, C.; Yune, S.; Tajmir, S. H.; Kim, M.; Do, S., Machine Friendly Machine Learning: Interpretation of Computed Tomography Without Image Reconstruction. *Sci Rep* **2019,** *9* (1), 15540.
231. Dong, J.; Fu, J.; He, Z., A deep learning reconstruction framework for X-ray computed tomography with incomplete data. *PLoS One* **2019,** *14* (11), e0224426.
232. Chen, H.; Zhang, Y.; Kalra, M. K.; Lin, F.; Chen, Y.; Liao, P.; Zhou, J.; Wang, G., Low-Dose CT With a Residual Encoder-Decoder Convolutional Neural Network. *IEEE Trans Med Imaging* **2017,** *36* (12), 2524-2535.

233. Schlemper, J.; Caballero, J.; Hajnal, J. V.; Price, A.; Rueckert, D. In *A Deep Cascade of Convolutional Neural Networks for MR Image Reconstruction*, Cham, Springer International Publishing: Cham, 2017; pp 647-658.
234. McCann, M. T.; Jin, K. H.; Unser, M., Convolutional Neural Networks for Inverse Problems in Imaging: A Review. *IEEE Signal Processing Magazine* **2017,** *34* (6), 85-95.
235. Yoo, J.; Sabir, S.; Heo, D.; Kim, K. H.; Wahab, A.; Choi, Y.; Lee, S. I.; Chae, E. Y.; Kim, H. H.; Bae, Y. M.; Choi, Y. W.; Cho, S.; Ye, J. C., Deep Learning Diffuse Optical Tomography. *IEEE Trans Med Imaging* **2020,** *39* (4), 877-887.
236. Ben Yedder, H.; BenTaieb, A.; Shokoufi, M.; Zahiremami, A.; Golnaraghi, F.; Hamarneh, G. In *Deep Learning Based Image Reconstruction for Diffuse Optical Tomography*, Cham, Springer International Publishing: Cham, 2018; pp 112-119.
237. Granda, J. M.; Donina, L.; Dragone, V.; Long, D. L.; Cronin, L., Controlling an organic synthesis robot with machine learning to search for new reactivity. *Nature* **2018,** *559* (7714), 377-381.
238. Li, Z.; Najeeb, M. A.; Alves, L.; Sherman, A. Z.; Shekar, V.; Cruz Parrilla, P.; Pendleton, I. M.; Wang, W.; Nega, P. W.; Zeller, M.; Schrier, J.; Norquist, A. J.; Chan, E. M., Robot-Accelerated Perovskite Investigation and Discovery. *Chemistry of Materials* **2020,** *32* (13), 5650-5663.
239. Vahrmeijer, A. L.; Hutteman, M.; van der Vorst, J. R.; van de Velde, C. J.; Frangioni, J. V., Image-guided cancer surgery using near-infrared fluorescence. *Nat Rev Clin Oncol* **2013,** *10* (9), 507-18.
240. Weissleder, R.; Pittet, M. J., Imaging in the era of molecular oncology. *Nature* **2008,** *452* (7187), 580-9.
241. Zhang, R. R.; Schroeder, A. B.; Grudzinski, J. J.; Rosenthal, E. L.; Warram, J. M.; Pinchuk, A. N.; Eliceiri, K. W.; Kuo, J. S.; Weichert, J. P., Beyond the margins: real-time detection of cancer using targeted fluorophores. *Nat Rev Clin Oncol* **2017,** *14* (6), 347-364.
242. Ntziachristos, V., Going deeper than microscopy: the optical imaging frontier in biology. *Nat Methods* **2010,** *7* (8), 603-14.
243. Helmchen, F.; Denk, W., Deep tissue two-photon microscopy. *Nat Methods* **2005,** *2* (12), 932-40.
244. Wang, L. V., Multiscale photoacoustic microscopy and computed tomography. *Nat Photonics* **2009,** *3* (9), 503-509.
245. Nguyen, Q. T.; Tsien, R. Y., Fluorescence-guided surgery with live molecular navigation--a new cutting edge. *Nat Rev Cancer* **2013,** *13* (9), 653-62.
246. Park, Y.; Jeong, S.; Kim, S., Medically translatable quantum dots for biosensing and imaging. *Journal of Photochemistry and Photobiology C: Photochemistry Reviews* **2017,** *30*, 51-70.
247. Resch-Genger, U.; Grabolle, M.; Cavaliere-Jaricot, S.; Nitschke, R.; Nann, T., Quantum dots versus organic dyes as fluorescent labels. *Nat Methods* **2008,** *5* (9), 763-75.
248. Probst, C. E.; Zrazhevskiy, P.; Bagalkot, V.; Gao, X., Quantum dots as a platform for nanoparticle drug delivery vehicle design. *Adv Drug Deliv Rev* **2013,** *65* (5), 703-18.
249. Hildebrandt, N.; Spillmann, C. M.; Algar, W. R.; Pons, T.; Stewart, M. H.; Oh, E.; Susumu, K.; Diaz, S. A.; Delehanty, J. B.; Medintz, I. L., Energy Transfer with Semiconductor Quantum Dot Bioconjugates: A Versatile Platform for Biosensing, Energy Harvesting, and Other Developing Applications. *Chem Rev* **2017,** *117* (2), 536-711.

250. Zhou, J.; Yang, Y.; Zhang, C. Y., Toward Biocompatible Semiconductor Quantum Dots: From Biosynthesis and Bioconjugation to Biomedical Application. *Chem Rev* **2015,** *115* (21), 11669-717.
251. Wegner, K. D.; Hildebrandt, N., Quantum dots: bright and versatile in vitro and in vivo fluorescence imaging biosensors. *Chem Soc Rev* **2015,** *44* (14), 4792-834.